# Department of Precision and Microsystems Engineering

Fatigue Based Topology Optimization of an Offshore Wind Turbine Drivetrain

Marek Slebioda

Report no   : 2023.018
Coaches   : Reinier Giele, Thomas Haex
Professor   : Matthijs Langelaar
Specialisation : Computational Design and Mechanics (CDM)
Type of report : MSc Thesis
Date   : March 30, 2023

TUDelft
Delft
University of
Technology

Challenge the future
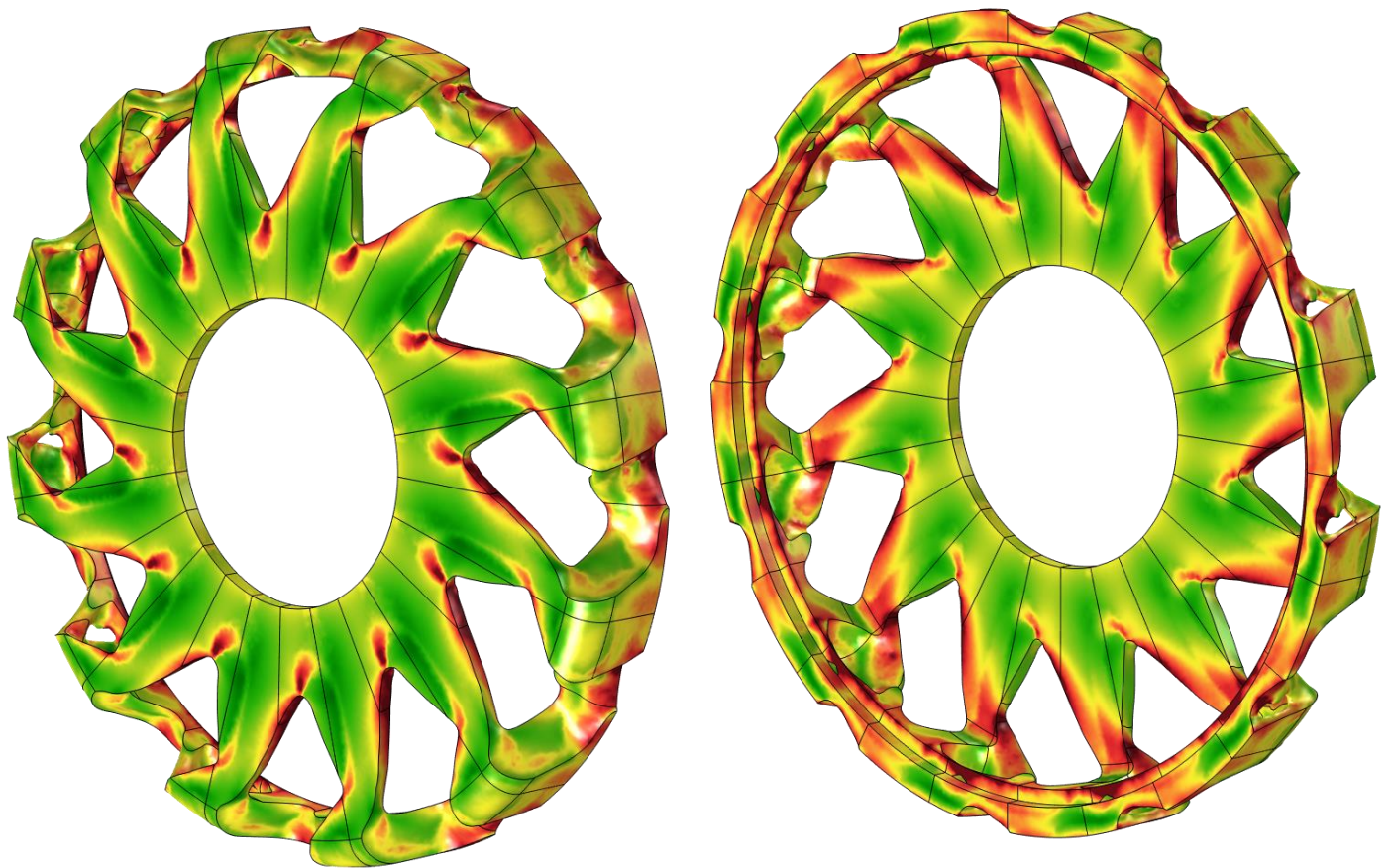
Fatigue Based Topology Optimization of an Offshore Wind Turbine Drivetrain

by

Marek Slebioda

to obtain the degree of Master of Science

at the Delft University of Technology,

to be defended publicly on March 30, 2023 at 11:00

This thesis is confidential and cannot be made public until March 30, 2025

An electronic version of this thesis is available at http://repository.tudelft.nl/.

TUDelft

Summary

Offshore wind turbines have seen a significant increase in size over the past decades. A critical consequence of this increase in size is a substantial increase in the torque transferred from the wind turbine rotor. This leads to the necessity of larger and heavier drivetrains to adhere to structural failure requirements and subsequently to larger and heavier tower and support structures increasing the total mass and cost of the turbine. Hence, reducing the mass-to-torque ratio of the drivetrain has become a key design challenge.

The company Delft Offshore Turbines (DOT) proposes to replace the conventional drivetrain in the top of the turbine with a hydraulic drivetrain, which has a lower mass-to-torque ratio. Although this concept shows promise, finding a low mass design that fulfils the infinite fatigue life requirement can be challenging. Using topology optimization to minimize mass while constraining the structural requirements could, therefore, be instrumental in the realization of this concept.

The design case by DOT can be classified as rotating machinery. In general rotating machinery is commonly subjected to periodic loading that varies non-proportionally in time. This results in fluctuating stresses causing material fatigue. A consequence of the non-proportionality of loading is that the time response needs to be computed to evaluate for fatigue, which adds additional computation cost. However, another common aspect found in rotating machinery is that parts are cyclic symmetric, which allows for a potential reduction in computation cost.

In this thesis a method is presented to implement infinite fatigue life constraints into density based topology optimization for structures subjected to non-proportional loading, while cyclic symmetric properties are exploited to reduce computation cost. It was found that when the load case on a cyclic symmetric part adheres to certain conditions, a single static FE-analysis can provide multiple time steps for a quasi-static analysis. Decreasing the computational burden roughly proportional to the unique number of time steps obtained. The largest local variations in stress are estimated using a smooth min/max function and aggregated into a global constraint.

The method was tested on several numerical problems as well as applied to the DOT design case. The results showed that the method was able to properly constrain a global fatigue constraint while minimizing mass, achieving final designs that might not be trivial to find by hand.

Preface

This preface marks the end of my thesis and a year filled with challenges. To whoever reads this I hope you find the work of interest and that it may inspire you for your own research. In spite of a master thesis project largely being a solo endeavour, it wouldn't have been possible without the help of people around me.

First of all I would like to thank my supervisors Matthijs and Reinier at the university, who were always available for questions when necessary. Their guidance has helped me obtain a deeper understanding of the topic and the feedback provided was always appreciated.

Special thanks to Thomas my supervisor at DOT, who's endless enthusiasm helped keep my spirits up when the road ahead seemed daunting. Our weekly meetings provided a healthy practical perspective on the research.

My appreciation also goes out to the other colleagues at DOT. For help provided, but mostly for the beers at Café Tango and the post work bouldering sessions.

At last I would like to express my gratitude towards my friends and family. My friends for providing necessary distractions at times with as highlight a long overdue trip to Cuba. And my family for their unconditional support.

This past year has been very instructive both educationally and personally. Now that it is over, the last thing I have to say is that I hope you enjoy reading the remainder of this report and that I'm looking forward to the new challenges ahead.

Marek Slebioda
Rotterdam, March 2023

Contents

1

Introduction

Offshore wind turbines have seen a significant increase in size over the past decades, as this improves the economy per system. Since the extracted power is proportional to the area covered by the rotor blades, an increase in rotor diameter leads to a quadratic increase in power. To avoid rapid decay of the wind turbine blades, however, the speed at the blade tips must be limited. This leads to a proportional decrease in rotation speed as rotor size increases. As the mechanical power produced by a wind turbine is the product of torque and rotation speed, the increase in size results in a cubic increase of the torque in the turbine. A consequence of the increased torque is the necessity of larger and heavier drivetrains to transfer loads while adhering to structural failure requirements. This increases the top-mass of the turbine, which subsequently leads to larger and heavier tower and support structures increasing the total mass and cost of the turbine. Hence, to reduce mass, converting large torque to useful energy whilst minimizing the mass-to-torque ratio has become a key drivetrain design challenge (DOT 2022).

A technological development by the company Delft Offshore Turbines (DOT), which focuses on Levelized Cost of Energy (LCOE) reduction of offshore wind energy, offers a potential path to this mass reduction. DOT proposes to replace the conventional drivetrain in the top of the turbine with a hydraulic drivetrain, which has a lower mass-to-torque ratio. The drivetrain is designed to operate at the same rotation speed and torque input as the turbine rotor without the need of a transmission. It transforms the kinetic energy in the turbine blades into hydraulic energy by pressurizing seawater. The pressurized seawater is used to generate power through a Pelton-generator on a central platform as shown in Figure 1.1. Multiple turbines can be coupled to this platform for collective power generation, which further contributes to LCOE reduction (DOT 2022).
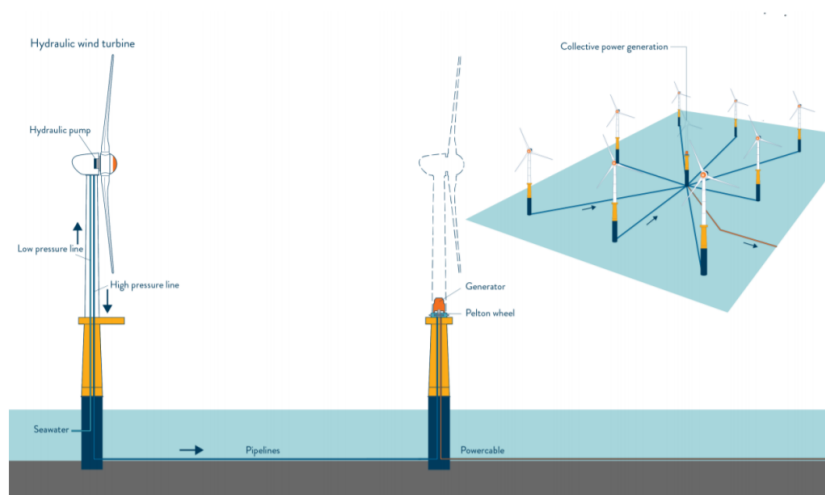

Figure 1.1: Hydraulic wind turbine concept of DOT (DOT 2022)

Although this concept shows promise, the large torque input and strict structural requirements can make it challenging to find a low mass design. Topology Optimization (TO), since its introduction by Bendsøe & Kikuchi (1988), has become a well-established design method for finding lightweight structures which adhere to a certain set of design constraints. Using TO to minimize mass while fulfilling the fatigue and stress requirements could, therefore, be instrumental in the realization of this concept.
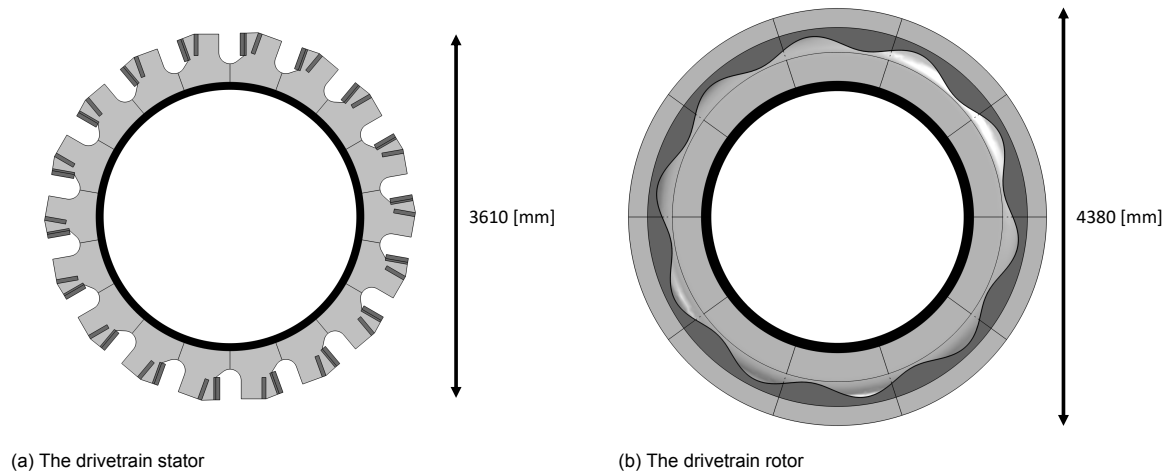
(a) The drivetrain stator

(b) The drivetrain rotor

In this research two large structural parts of the DOT hydraulic drivetrain are chosen as a case study for mass minimization. The first part is the drivetrain stator, as illustrated in Figure 1.2b, which consists of a ring with a number of flanges. The flanges provide linear guidance to rollers moving back and forth radially. The tangential forces are transferred to the fixed inner ring. The second part is a casing that transfers an input torque at the inner ring, which is radially constrained, to a number of rollers through a camring, as illustrated in Figure 1.2b. By analysing the design cases, three aspects that render them unique were identified:

- The parts are to be designed for infinite fatigue life.

- The parts are subjected to periodic surface loads which change in magnitude as well as position in time.

- The parts are dividable in cyclic symmetric segments.

These aspects have been studied separately in TO literature. The combination of fatigue and the non-proportionality of the type of loading, however has not been sufficiently studies for infinite fatigue life constraints. The consequence of this combination is that a time-varying stress history needs to be computed, as the maximum and minimum stress in time needs to be ascertained at every point in the design domain. This significantly increases the computational cost of the FE-analysis. Therefore, combining this method with a procedure that exploits cyclic symmetric properties to reduce computational cost, is certainly relevant to explore. A suitable method which combines the different aspects is lacking in existing literature and combining different TO approaches is known to often be nontrivial. This thesis, therefore, aims to present a method for problems of this nature, which leads to the research question:

> *How can time-varying periodic loading and cyclic symmetry be combined for fatigue constrained TO?*

In order to answer this, the following sub questions are answered:

- *How can fatigue be incorporated in TO for non-proportional time-varying loading?*

- *To what extent can taking non-proportionality of loading into consideration improve constraint adherence of the optimized result?*

- *How can cyclic symmetry be exploited to reduce the computational cost of the optimization problem?*

The main matter of this thesis is a written article on the method developed to combine the different aspects mentioned, which is presented in Chapter 3. Some additional background information on topology optimization and specifically stress based TO is provided in Chapter 2. The resulting method is discussed and conclusions are drawn in Chapter 5. In Appendix A some less straight forward implementation approaches in COMSOL are shown and in Appendix B some supplementary results considering mesh size and filter radius are presented.

<div align="right">

2

</div>

Background Topology optimization

2.1. Topology optimization

Topology optimization is part of a set of structural optimization methods. Bendsøe & Sigmund (2003) distinguish the following three categories: sizing, shape and topology optimization (as illustrated in Figure 2.1). Sizing optimization is typically used when structural members are optimized using a single sizing parameter, for instance the cross sectional area of a truss. The limitation to this method is that a ground structure needs to be defined pre-emptively. Shape optimization is more free in optimizing a geometry. It takes as starting point a parameterized predefined topology and uses the parameters to optimize its shape. Both these methods need a priori assumptions about the optimal topology, resulting in optimized designs that can be highly dependent on the initial assumptions. Topology optimization does not need these assumptions. It distributes material within a defined design domain, adding or removing material freely where necessary. This makes TO the most versatile structural optimization method.
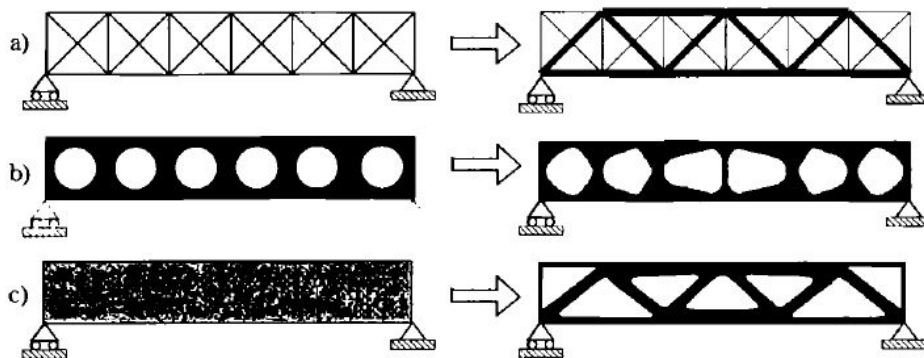
Figure 2.1: Different structural optimization approaches. a) Sizing optimization, b) shape optimization and c) topology optimization (Bendsøe & Sigmund 2003).

2.2. Stress constraints

Stress based topology optimization introduces two main challenges into the optimization. The first one is the so called "singularity" problem, which is caused by stress constraints vanishing when design variables go to zero density. The second one is that stress is a local variable. Constraining the maximum stress on a domain results in a large set of local constraints, which makes the computation of sensitivities expensive, due to a loss in the efficiency of the adjoint method. Both these issues are discussed further in the following sections.

2.2.1. Stress relaxation

The singularity problem was observed by Cheng & Jiang (1992) when including stress constraints in a truss optimization problem. It is caused by stress constraints discontinuously jumping to zero when one of the design variables reaches zero density as shown in Figure 2.2. This results in a part of the design domain being of a lower dimension known as a degenerate subdomain. The desired optimum can reside in this subdomain and is called a singular optimum. Gradient based optimization algorithms cannot reach this subdomain and will converge to a different local optimum.

This issue can be resolved using constraint relaxation methods, which smooth the discontinuous point of the stress constraint so that the degenerate subdomain is reunited to the rest of the feasible domain. Methods like ϵ-relaxation (Cheng & Guo 1997)(Duysinx & Bendsøe 1998) and qp-relaxation (Bruggi 2008)(Le et al. 2010), have been shown to successfully deal with this issue.
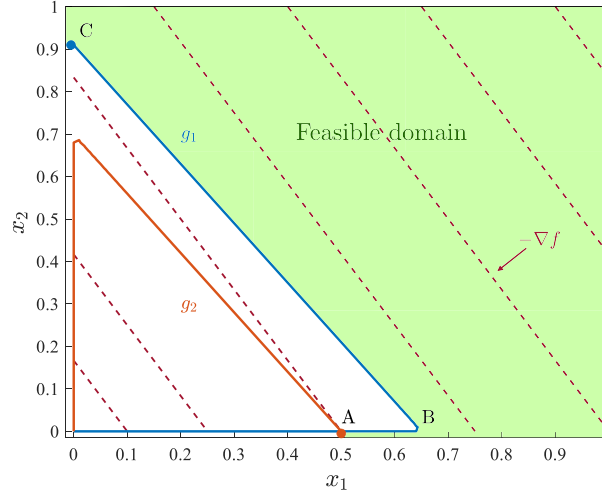

Figure 2.2: The design domain of a stress constrained optimization problem with two design variables x_1 and x_2 and two stress constraints g_1 and g_2. The dashed lines represent levels of the objective function f. Point A is a singular optimum and in this case also the global optimum. Point B is a discontinuous point of constraint g_1. Point C is a local optimum. The domain between point A and B is a degenerate subdomain.

2.2.2. Constraint aggregation

The issue of the large set of local constraints can be dealt with by combining them into a single global constraint. This has been done with the use of aggregation functions like the p-norm (Duysinx & Sigmund 1998) shown in Equation 2.1 and Kresselmeier–Steinhauser (KS) function (Yang & Chen 1996) shown in Equation 2.2, which approximate the maximum local variables in a smooth, thus differentiable, manner. These functions introduce an aggregation parameter k, which determines the accuracy of the approximation. When k goes to infinity, the approximation will approach the true maximum. For finite values of k, the functions will overestimate the true maximum. These functions are turned into a smooth minimum approximation by using a negative value for k. In this case the approximated minimum is smaller than the true minimum.

$$\sigma_{\max}^{\mathrm{PN}} = \left(\sum_{i \in \Omega} (\sigma_i(x))^k \right)^{\frac{1}{k}} \geq \max_{i \in \Omega} \sigma_i(x), \qquad \sigma_{\min}^{\mathrm{PN}} = \left(\sum_{i \in \Omega} (\sigma_i(x))^{-k} \right)^{\frac{1}{-k}} \leq \min_{i \in \Omega} \sigma_i(x) \qquad (2.1)$$

$$\sigma_{\max}^{\mathrm{KS}} = \frac{1}{k} \ln \left(\sum_{i \in \Omega} e^{k\sigma_i(x)} \right) \geq \max_{i \in \Omega} \sigma_i(x), \qquad \sigma_{\min}^{\mathrm{KS}} = \frac{1}{-k} \ln \left(\sum_{i \in \Omega} e^{-k\sigma_i(x)} \right) \leq \min_{i \in \Omega} \sigma_i(x) \qquad (2.2)$$

3

Article: Topology optimisation for infinite fatigue life of cyclic symmetric structures subjected to non-proportional loading

Topology optimization for infinite fatigue life of cyclic symmetric structures subjected to non-proportional loading

Marek Slebioda

Abstract

This paper presents a density based topology optimization method for infinite fatigue life constraints of non-proportional load cases, with a specific focus on parts with cyclic symmetry. Considering non-proportional loads into topology optimization significantly broadens the types of design problems that can be handled. The method estimates the local variation in signed von Mises stress using a smooth min/max function and constrains the resulting stress amplitude using established stress based topology optimization methods. Accounting for non-proportionality of loading significantly increases the computation cost with respect to existing proportional methods, as the time-varying stress field needs to be computed. Inertia effects are neglected in the structural analysis. Therefore, a quasi-static analysis is used to obtain the stress history. To reduce the computational cost advantage is taken of cyclic symmetric properties to reduce the number of necessary time steps to evaluate. This reduces the computational cost roughly proportional to the number of unique load time steps present in the repeated segments as opposed to a standard implementation. The method is tested on numerical examples in 2D and 3D for both proportional and non-proportional loads and was found to be locally accurate up to the accuracy of the aggregation over the relaxed constraints.

Keywords: Topology optimization, Fatigue constraints, Non-proportional loading, Cyclic symmetry

---

1. Introduction

Rotating machinery is a common sight in industrial applications (Rao, 2011). Due to relative rotation between a part and its loading, the load case generally varies periodically in time, resulting in fluctuating stresses in the material. These fluctuations cause material fatigue even for stresses below the yield stress of the material. Fatigue failure as opposed to static failure is, therefore, often the critical failure constraint for dynamically loaded structures. The life time of a part with respect to material fatigue is dependent on the magnitude and amount of load cycles it is subjected to. For parts where a long lifetime is desired, for example due to costly or inconvenient replacement, a requirement can be that the part should be designed for infinite fatigue life. This constraint can be conflicting with other design requirements like minimizing the material usage of the part to reduce weight, inertia or cost. While in some cases a proportional load case applies, many applications are subjected to a non-proportional load case like moving loads or out of phase loads. This has implications for both the structural analysis and choice of fatigue criterion, which substantially increase the computational cost. Another common aspect of rotating parts subjected to periodic loading, however, is the presence of cyclic symmetry in the design, which can result from cyclic symmetry in the load case or possibly for manufacturing reasons. This symmetry can often be exploited to reduce the computation cost of the structural analysis.

Finding a low mass design while fulfilling the structural requirements can be challenging. Density based Topology Optimization (TO) has become a well-established design
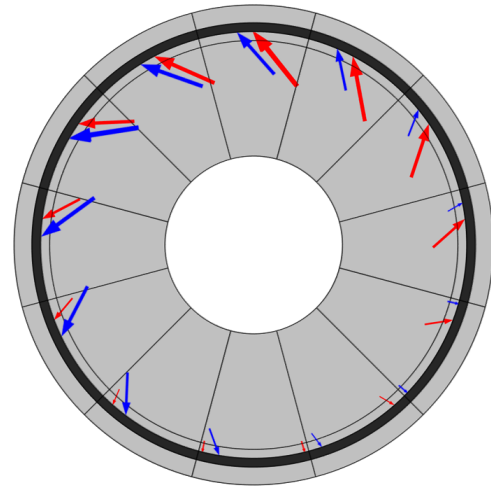

Figure 1: A design problem combining the three key aspects of this paper. The gray design region consists of twelve cyclic symmetric segments and must be designed for infinite fatigue life while minimizing material usage. The loads vary periodically in position and magnitude around the circumference

method for finding lightweight structures which adhere to a certain set of design constraints. Using TO to minimize for mass while constraining fatigue and exploiting cyclic symmetry could be very useful for rotating machinery design.

TO methods separately considering infinite fatigue life, time-varying non-proportional loading and cyclic symmetry have been proposed previously. However, a suitable method which combines them is lacking in existing literature. This paper, therefore, aims to present a TO method that can be used to

design parts like illustrated in Figure 1 containing the following aspects:

- The part is to be designed for infinite fatigue life.

- The part is subjected to periodic loads which vary non-proportionally in time.

- The part is dividable in a number of cyclic symmetric segments.

Below the state of the art regarding each individual aspect is briefly reviewed and choices are motivated, before the contributions of this paper are stated.

1.1. Fatigue based TO

Fatigue failure is caused by subjecting a structural component to dynamic loading conditions. Even though resulting stresses can be well below the static failure criteria, the component will break due to material fatigue after a certain amount of loading fluctuations. To evaluate the expected fatigue life of a structural component, different approaches can be considered: crack propagation rate, strain-life and stress-life. Crack propagation rate approaches are used to estimate the propagation of surface cracks through the material after crack initiation and therefore more commonly used for finite lifetime applications. Strain-life is commonly used for short lifetime applications where plastic deformations occur. For longer lifetime applications, including infinite lifetime, a stress-life approach is commonly used (Lalanne, 2014). The majority of existing fatigue based TO research is based on a stress-life approach. For these reasons a stress-life approach is used in this paper.

Stress-life fatigue analysis looks at the variations in stress caused by the dynamic loading. These stress fluctuations, called stress cycles, can then be interpreted to an expected life time using an SN-diagram, for illustration shown in Figure 2. Three approximate regions can be distinguished in the SN-diagram, the first region being for low-cycle fatigue which is characterised by plastic deformations. The second region is for high-cycle, but finite fatigue life. The third region is for infinite fatigue life (Lalanne, 2014). Some loading might result into stress fluctuations where defining stress cycles is non-trivial. A Rainflow counting method (Amzallag et al., 1994) can then be used to dissect the complicated fluctuations into a combination of stress cycles and Palmgren-Miner rule can be used to evaluate the accumulative fatigue damage (Lalanne, 2014). It is important to note that SN-diagrams are based on experimental data and are only valid for uniaxial and zero mean stress cases. When this is not the case, correction methods are necessary. Methods like the signed von Mises stress, largest principal stress direction and critical plane methods are commonly used in fatigue analysis for defining an equivalent uniaxial stress from a multiaxial stress state (Carpinteri et al., 2017). For mean stress correction the Modified Goodman, Soderberg or Gerber corrections can be used (Lalanne, 2014).

Since a stress-life fatigue approach is based on stress fluctuations, fatigue based TO problems are closely related to
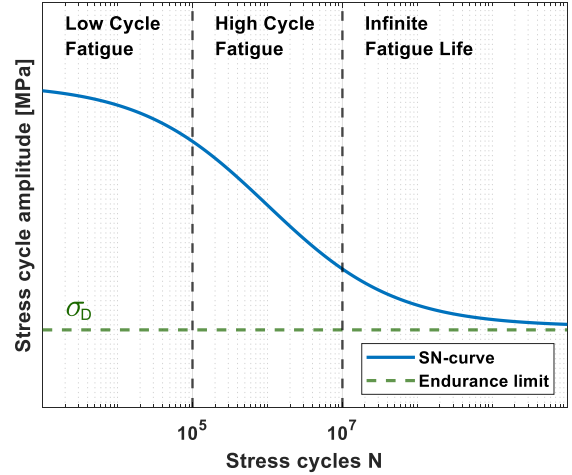

Figure 2: A general representation of an SN-diagram. It shows an approximation of the expected amount of lifetime in number of cycles N for a given stress cycle amplitude. Some materials, like most steel types, have an endurance limit σ_D below which no fatigue damage occurs.

stress based TO and evidently the same problems arise as have been observed with stress based TO.

One of these problems is the so called "singularity" problem, which was observed by Cheng and Jiang (1992) when including stress constraints in a truss optimization problem. It is caused by stress constraints vanishing when one of the design variables reaches zero density. This results in a part of the design domain being of a lower dimension known as a degenerate subdomain. The desired optimum can reside in this subdomain and is called a singular optimum. Gradient based optimization algorithms cannot reach this subdomain and will converge to a different local optimum.

This can be resolved using constraint relaxation methods, which smooth the discontinuous point of the stress constraint so that the degenerate subdomain is reunited with the rest of the feasible domain and can be reached by the optimization algorithm. Methods like ϵ-relaxation (Cheng and Guo, 1997; Duysinx and Bendsøe, 1998) and qp-relaxation (Bruggi, 2008; Le et al., 2010), have been shown to successfully deal with this issue.

A second difficulty is the local nature of stress and fatigue. The constraint should be satisfied everywhere in the design domain. This gives a large set of local constraints, which makes the computation of sensitivities expensive, as the efficiency of the adjoint method used for the sensitivity analysis is lost.

This problem can be dealt with by aggregating the many local constraints into a single global constraint. This has been done with the use of aggregation functions like the p-norm (Duysinx and Sigmund, 1998) and the Kresselmeier–Steinhauser (KS) function (Yang and Chen, 1996), which approximate the maximum local constraint value in a differentiable manner, where the accuracy of the approximation is controlled with an aggregation parameter. For large aggregation parameters, however, the global constraint becomes unstable. To improve the inaccuracy of the approximation, Le et al. (2010) proposed

a global constraint scaling measure, that uses the true and approximated maximum stress of the previous optimization iteration to scale the approximation of the current iteration. In Verbart et al. (2017), a unified aggregation and relaxation method is proposed to deal with both the local constraints and singularity problem simultaneously using a single aggregation parameter. This was done by introducing a lower bound version of the p-norm and KS-function aggregation.

A disadvantages of aggregation methods is a loss in local stress control as well as the accuracy of the approximation being problem and mesh size dependent. Recent studies have, therefore, proposed the use of the Augmented Lagrangian (AL) method to handle the local stress constraints (Senhora et al., 2020; da Silva et al., 2021a). The AL method treats the stress constraints as a local quantity by adding them to the objective function in the form of a penalty term, which is updated at each iteration. This unconstrained problem is expected to converge to the solution of the original constrained problem, but requires only a single adjoint vector in the sensitivity analysis. The local stress control of the AL method was shown to be significantly better than global constraint approaches by da Silva et al. (2021a).

Previous studies have successfully incorporated fatigue into TO. Holmberg et al. (2014) were the first to incorporate the methods from stress based TO and apply them to a fatigue based problem. The fatigue analysis is performed in advance of the optimization by computing the largest allowable stress amplitude for which the accumulative damage, for a known load spectrum, is not exceeded. This stress amplitude is then incorporated like a stress constraint. Oest and Lund (2017) takes a similar approach, but incorporates the fatigue analysis into the optimization problem directly, by constraining the accumulative damage function. Jeong et al. (2015) consider infinite fatigue life for zero-mean harmonic loading in steady state. The mean stress is computed from a static analysis of the mean load and the amplitude stress from a harmonic analysis of the load amplitude. They employ a SIMP like interpolation scheme on the mass matrix, with the aim to avoid localized mode issues. Furthermore, they provide differentiable versions of some commonly used mean stress correction methods. Collet et al. (2017) incorporates the mean stress correction in a different manner by implementing the endurance envelope of the modified Goodman correction as separate stress constraints. Furthermore, they use an active constraint set to limit the number of local constraints considered instead of aggregating them into one constraint. Since the amount of active constraints changes during the optimization, a global compliance constraint is introduced to smooth any discontinuities. Lee et al. (2015) consider fatigue constraints for a stochastic load case and utilises and compares frequency based fatigue analysis methods. Jeong et al. (2018) perform a transient analysis to acquire the time-varying stress history caused by variable amplitude loading. A multiaxial cycle counting method by Wang and Brown (1996) is used to extract effective stress cycles. Since the computation of transient sensitivities is expensive, they are computed from the

equivalent static load (Kang et al., 2001) at discrete time steps.

The fatigue constraint studies discussed so far have only considered proportional load cases. This is computationally advantageous, as the stress history can be obtained by linearly scaling the stress field from a single reference load. For non-proportional load cases, like moving loads or out of phase loads, the time response cannot be obtained in this manner and these methods will therefore not suffice.

Recent contributions have proposed fatigue based TO methods which involve non-proportional load cases. Zhang et al. (2019) propose that the non-proportional loading can be decomposed into a linear combination of unit loads with time varying weight factors. The stress history can then be constructed by summing the resulting unit stress fields multiplied by the corresponding time varying weight factors. From the stress history, the equivalent signed von Mises stresses are computed and rainflow counting is used to extract stress cycles at every element in the design domain. Suresh et al. (2020) use a continuous time fatigue analysis method developed by Ottosen et al. (2008) to approximate the evolution of damage at each element using differential equations. An endurance surface is defined in the stress space, which evolves depending on the current stress and a back stress tensor. Damage is accumulated when the stress state is outside of the endurance surface while it is evolving.

In this paper an alternative approach is presented to deal with non-proportional load cases. Since the goal is to design for infinite fatigue life, the fatigue analysis can be simplified to determining whether the amplitude of the largest stress cycle is below the endurance limit. Therefore, a smooth min/max function is used to approximate the local stress extrema in time, which defines the largest stress cycle locally. These local stress cycles are constrained using the stress constraint formulations presented in Bruggi (2008) and Verbart et al. (2017).

1.2. Time-varying TO

To obtain the time response of a structure under non-proportional loading, three types of approaches can be considered:

1. Quasi-static analysis
2. Transient analysis
3. Frequency response analysis

Previous studies have successfully implemented these approaches for different time-varying TO problems. The aforementioned approach by Zhang et al. (2019) and the Equivalent Static Load (ESL) method by Kang et al. (2001) are examples of a quasi-static analysis. The ESL is defined as a static load that would results in the same displacement field caused by a time-varying load at a chosen time point. Choi and Park (2002) used an approximate version of the ESL method to obtain the quasi-static time response for all time intervals.

For the transient analysis approach, time integration of the Equations of Motion (EoM) is required. Giraldo-Londoño and Paulino (2021b) have implemented the HHT-α integration scheme by Hilber et al. (1977), which is based

on a Newmark integration method, to solve time-varying compliance minimization problems. Time integration is a computationally expensive approach for TO problems. To reduce the computational burden, model reduction methods can be used to transform the EoM's into a reduced set of uncoupled equations, which can be solved more efficiently. Either modal DoF's or Ritz vectors can be used to replace the nodal DoF's as a base of the EoM's (Cook et al., 2002).

These model reduction methods can also be used for frequency response analysis. The frequency response gives the response of a DoF to harmonic excitation forces. It is computationally more efficient than time integration, but is limited to forces that can be expressed as a sum of Fourier series components, meaning that the forces should be periodic (Cook et al., 2002). Studies by Yoon (2010) and Liu et al. (2015) have investigated the accuracy and advantages of using model reduction methods for frequency response analysis in dynamic compliance minimization problems.

The main purpose for implementing the ESL method, transient analysis or frequency response analysis is usually to incorporate the dynamics of accelerating masses or vibrations. For this paper, these dynamic effects are not deemed relevant and therefore not considered. A quasi-static analysis similar to the approach used by Zhang et al. (2019) will therefore be used to obtain the time-varying stress history.

1.3. Cyclic symmetry

Many studies have exploited symmetry and periodicity to reduce the computational burden of solving optimization problems. An often considered example is the "MBB-beam", where instead of optimizing the entire beam, half the beam is modelled and a boundary condition is added to represent the symmetry.

In other cases, the design problem itself might not be symmetric, but a design requirement could be that the resulting geometry is. Kosaka and Swan (1999) proposed a method to enforce symmetry into the design by combining the densities of symmetrically corresponding elements into one design variable. A similar approach was used by Huang and Xie (2008) and Zuo (2009) for problems containing finite periodic cells. They average the sensitivities of corresponding elements to enforce periodicity. For infinitely periodic problems, where the load case is equivalent between periodic cells, Barbarosie and Toader (2010) used a periodic boundary condition. This links the nodes of corresponding periodic boundaries and reduces the structural analysis to a single Representative Unit Cell (RUC).

An equivalent way to formulate cyclic symmetry is as periodically repeating segments in tangential direction. Moses et al. (2002) studied periodic compliant minimization problems where the loads do not adhere to the periodicity of the geometry. They made use of the Discrete Fourier Transform (DFT) to solve the boundary value problem. Due to the specific nature of the DFT, this method is limited to infinitely periodic problems and complex numbers arise in the computation. Thomas (1979) presents two approaches to reduce the FE-analysis to a RUC for cyclic symmetric problems, where the periodic loading

between segments is shifted in time. The first is through modal analysis, where the periodicity is described by mode shapes containing complex numbers. The second is by describing the periodic loading using complex numbers. Petrov (2004) uses the complex mode shape approach and performs a frequency response analysis.

This paper considers load cases where each cyclic symmetric segment is subjected to the same load case. The load case of each segment, however, is out-of-phase with respect to the other segments. Therefore, the complete load case does not follow the cyclic symmetry of the geometry at a single point in time. The approaches by Moses et al. (2002), Thomas (1979) and Petrov (2004) are capable of reducing the structural analysis of such a problem to a single segment. however, the introduction of complex numbers has a higher computational cost. Therefore, in this paper a different approach is chosen. The cyclic symmetry is enforced similarly to the method used by Kosaka and Swan (1999), where the full structure is modeled. The disadvantage of not reducing the FE-analysis, however, is mitigated by combining it with the quasi-static analysis as will be explained further in Section 2.4.

1.4. Contribution

This paper presents a method to incorporate infinite fatigue life constraints into topology optimization of structures subjected to non-proportional loading. The largest stress cycle is determined using a smooth min/max function on the time-varying signed von Mises stress obtained from a quasi-static analysis. The method is combined with an approach to enforce cyclic symmetry in the design. This combination is of interest, as it can significantly reduce the computational cost of the quasi-static analysis when the loading adheres to the following conditions:

1. The loading is periodic.
2. Each segment is subjected to the same loading over one time period.
3. Between segments exists a constant shift in time over the loading period.

When these conditions are met, a single static analysis of the structure can represent multiple time steps of the quasi-static analysis. Types of loading that follow these conditions are load cases that appear to act like a traveling wave around the axis of symmetry, which is not uncommon in rotating machinery.

The presented fatigue constraint approach is first tested independently on three numerical examples, where a comparison is made to proportional approximations of the problems. This is meant to illustrate the relevance of taking non-proportionality of loading into consideration. The combination of the method with cyclic symmetry is thereafter tested on a 2D and a 3D example.

The results are validated for fatigue using both the signed von Mises method and Dang Van critical plane method (Karolczuk et al., 2016). A comparison is made to identify weaknesses of using the signed von Mises stress as equivalent fatigue stress.

4

The remainder of the paper is structured as follows. In Section 2 first the density based TO method used is explained and subsequently the proposed method is presented. The analysed fatigue test problems including the cyclic symmetric problems are introduced in Section 3 and the results of the problems are presented in Section 4 and thereafter discussed. Finally, conclusions are drawn in Section 5.

2. Methodology

2.1. Density based topology optimization

The objective in the considered design problems is to minimize the mass of the structure, while adhering to a global infinite fatigue life constraint. An equivalent interpretation is to minimize the material volume V used within the design domain, which is normalised with respect to the total volume V_Ω of the design domain. Density based TO will be used to achieve this. The domain is partitioned into finite elements, where an artificial density design variable $\rho_e \in [0, 1]$ is assigned to each element e. A density of 1 represents a volume element containing material, while a density of 0 represents a void volume element. The isotropic material properties of the finite elements are made dependent on these design variables in a continuous manner, such that the global structural performance with respect to the design variables can be analysed.

Since the fatigue constraint g_G^f only constrains the fluctuations in stress, which can allow for stresses above the yield stress, an additional global stress constraint g_G^s is necessary to constrain the static yield requirements of the structure, resulting in the following optimization problem:

$$\mathbb{P} : \min_\rho \quad V = \frac{1}{V_\Omega} \sum_{e \in \Omega} \bar{\rho}_e v_e,$$
$$\text{s.t.} \quad g_G^f \le 0,$$
$$g_G^s \le 0, \quad (1)$$
$$0 \le \rho \le 1,$$

where V_Ω is the volume of the design domain Ω, v_e is the volume of a finite element and $\bar{\rho}_e$ is the projected density field, which will be discussed further in Section 2.2.

The iterative optimisation works as follows: a FE-analysis is performed on an initial design to acquire the displacements and stress field of the structure from which the constraint values and objective function are evaluated. This is followed by a sensitivity analysis of the constraints and objective function with respect to the design variables. The gradients and function values are used to update the design variable values for the next iteration.

The density based method used is the modified SIMP method by Sigmund (2007). It applies a penalization function, $\eta_K(\bar{\rho}_e) = \bar{\rho}_e^p$, on the Young's modulus E_0 used to construct the elemental stiffness matrices $\mathbf{K}_e$ as follows:

$$E_e(\bar{\rho}_e) = E_{\min} + \eta_K(\bar{\rho}_e)(E_0 - E_{\min}), \quad (2)$$

where $E_e(\bar{\rho}_e)$ denotes the effective Young's modulus. The penalization variable p is chosen such that the elemental

stiffness gained from intermediate densities is low relative to the amount of mass gained. This is achieved for values of $p > 1$. A common choice is $p = 3$, which is also used for this paper and for which the interpolation is shown in Figure 3. To avoid singularity of the global stiffness matrix $\mathbf{K}(\bar{\rho})$, a lower bound value $E_{\min} = 10^{-9}E_0$ is assigned to the effective Young's modulus. The global stiffness matrix is assembled from the elemental stiffness matrices $\mathbf{K}_e$ as follows:

$$\mathbf{K}(\bar{\rho}) = \sum_{e \in \Omega} \mathbf{K}_e(E_e(\bar{\rho}_e)). \quad (3)$$

An underlying constraint of the optimization problem is that the solution should satisfy the static equilibrium equations:

$$\mathbf{K}(\bar{\rho})\mathbf{u}(\bar{\rho}, t_i) = \mathbf{f}(t_i), \quad i = 1, .., N, \quad (4)$$

where $\mathbf{u}$ is the nodal displacement vector and $\mathbf{f}$ is the vector containing the external forces. This is implemented through the FE-analysis step. A time-varying stress history needs to be determined for fatigue analysis, while inertia effects can be neglected. A quasi-static FE-analysis is, therefore, performed at discrete time steps t_i. The number of time steps N is an important consideration. In this paper the number of time steps used is chosen intuitively for the individual examples. The choice is based on the range of motion of the load and its variation in magnitude, making sure that points of interest such as load and motion extrema are included.

2.2. Distributed density formulation

The design variables ρ are connected to the density distribution field $\bar{\rho}$ through a density filter and threshold projection. The density filter works like a blurring filter causing a gray transition between material and void regions in the design domain. It avoids mesh dependency of the solution and introduces control over minimal feature size. The gray transition region is also necessary for stress based problems to avoid high local stresses along jagged material boundaries.
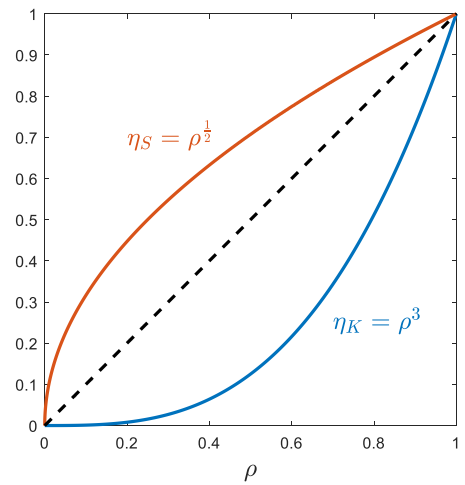

Figure 3: Interpolation functions used for the Young's modulus (η_K) and stress (η_S).

5

The density filter used is a Partial Differential Equation (PDE) based filter (Lazarov and Sigmund, 2011) and gives the density filtered field $\tilde{\rho}$ according to:

$$\tilde{\rho} = \rho - R_{\text{PDE}}^2 \nabla^2 \tilde{\rho}. \tag{5}$$

Here, R_{PDE} is the filter radius. Unless specified otherwise, the filter radius is set to $R_{\text{PDE}} = 1.5\, l_e$, where l_e is the average element size.

A threshold projection subsequently controls the gray transition region and relates the filtered density field to the projected field using a Heaviside projection function (Wang et al., 2011):

$$\bar{\rho} = \frac{\tanh(\beta\eta) + \tanh(\beta(\tilde{\rho} - \eta))}{\tanh(\beta\eta) + \tanh(\beta(1 - \eta))}. \tag{6}$$

Here, η is the projection threshold and is set to 0.5. The steepness of the projection function and therefore the width of the gray transition region is controlled by the parameter β. In da Silva et al. (2021b) an upper bound on β for stress based optimization problems using the given PDE filter is defined. The upper bound ensures a minimum transition width of one element and is given as $\beta_{\text{lim}} = \frac{2R}{l_e\sqrt{3}}$, where R is the filter radius of the classical linear hat function by Bruns and Tortorelli (2001), which is related to R_{PDE} according to $R = 2\sqrt{3}R_{\text{PDE}}$ (Lazarov and Sigmund, 2011). For the filter radius used this results in $\beta_{\text{lim}} = 6$.

2.3. Infinite fatigue life constraint

When the stress history is acquired from the quasi-static analysis, the largest stress cycle needs to be identified for the fatigue evaluation. The signed von Mises stress is used as equivalent stress measure. First, however, the singularity problem as mentioned in the introduction needs to be dealt with. This is done by using the qp-relaxation approach by Bruggi (2008) as applied by Lee et al. (2015). Giving the von Mises stress interpolation function η_S as follows:

$$\eta_S(\bar{\rho}_e) = \frac{\eta_K(\bar{\rho}_e)}{\bar{\rho}_e^q} = \bar{\rho}_e^{(p-q)}. \tag{7}$$

Choosing a stress interpolation parameter $q < p$ relaxes the stress for intermediate densities and resolves the singularity problem. A value of $q = 2.5$ is chosen, giving the interpolation function $\eta_S(\bar{\rho}_e) = \bar{\rho}_e^{\frac{1}{2}}$ shown in Figure 3 and the relaxed stress computation:

$$\hat{\sigma}_e(\bar{\rho}_e, t_i) = \eta_S(\bar{\rho}_e)\mathbf{C}_e\epsilon_e(t_i). \tag{8}$$

Here, $\hat{\sigma}_e$ is the relaxed stress, $\mathbf{C}_e$ the elasticity tensor based on the non-penalised Young's modulus and $\epsilon_e(t_i)$ the infinitesimal strain at time step i.

The signed von Mises stress is computed from the relaxed stress as shown in Equation 9, where $\mathbf{J}_2$ is the second invariant of the deviatoric stress tensor. The sign is determined from the sign of the hydrostatic stress σ_e^{H}. Since the sign operator is discontinuous at 0, it is replaced by the hyperbolic tangent function tanh, which acts as a smooth sign function.

$$\tilde{\sigma}_e(\bar{\rho}_e, t_i) = \tanh(\sigma_e^{\text{H}}(t_i)) \sqrt{3\mathbf{J}_2(\hat{\sigma}_e(\bar{\rho}_e, t_i))}. \tag{9}$$

For an infinite fatigue life constraint, the fatigue life analysis can be reduced to whether the largest stress cycle in the stress history of each element is below the endurance limit σ_D and no complex cycle counting method is required. The largest stress cycle is determined by approximating the maximum $\sigma_e^{\text{max}}(\bar{\rho}_e)$ and minimum $\sigma_e^{\text{min}}(\bar{\rho}_e)$ signed von Mises stress in time using the upper bound KS-function as follows:

$$\sigma_e^{\text{max}}(\bar{\rho}_e) = \frac{1}{k_1} \ln\left(\sum_{i=1}^{N} e^{k_1\tilde{\sigma}_e(\bar{\rho}_e, t_i)}\right). \tag{10}$$

$$\sigma_e^{\text{min}}(\bar{\rho}_e) = \frac{1}{-k_1} \ln\left(\sum_{i=1}^{N} e^{-k_1\tilde{\sigma}_e(\bar{\rho}_e, t_i)}\right). \tag{11}$$

The KS-function is chosen over the p-norm, because the latter cannot distinguish negative from positive input values. The aggregation parameter k_1 controls how much the function will overestimate the true maximum and minimum. A value of $k_1 = 20$ is chosen. From the maximum and minimum stresses the mean and amplitude stress of the largest stress cycle are computed according to:

$$\sigma_e^{\text{m}}(\bar{\rho}_e) = \frac{\sigma_e^{\text{max}}(\bar{\rho}_e) + \sigma_e^{\text{min}}(\bar{\rho}_e)}{2}. \tag{12}$$

$$\sigma_e^{\text{a}}(\bar{\rho}_e) = \frac{\sigma_e^{\text{max}}(\bar{\rho}_e) - \sigma_e^{\text{min}}(\bar{\rho}_e)}{2}. \tag{13}$$

Mean stress can have a negative effect on the fatigue life. To correct for the mean stress, the modified Goodman method, as illustrated in Figure 4, is applied. Since only the tensile mean stress is assumed to negatively impact the fatigue life, the correction is non-smooth at $\sigma_e^{\text{m}}(\bar{\rho}_e) = 0$. For this reason
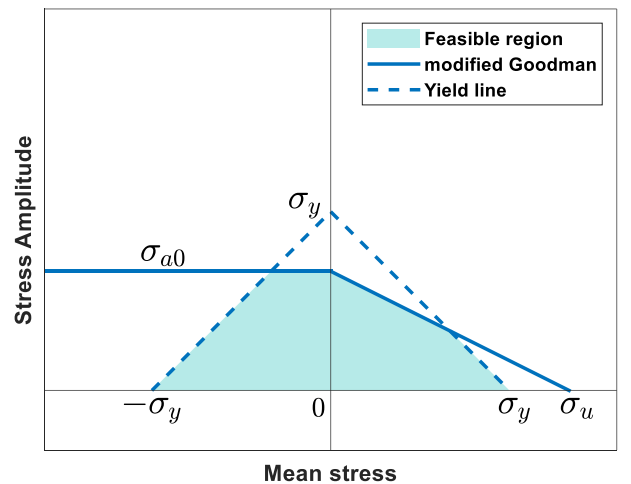

Figure 4: The effect of mean stress on the allowable stress amplitude according to the modified Goodman correction method. $\sigma^{\text{a}0}$ is the stress amplitude at zero mean stress, σ_{Y} is the yield stress and σ_{U} is the ultimate tensile stress of the material. The combination of fatigue and static yield criteria define an endurance envelope which constrains a feasible region.

the differentiable modified Goodman approach by Jeong et al. (2015) is used, which puts all negative mean stresses to zero in a differentiable manner as follows:

$$\sigma_e^{\mathrm{m0}}(\bar{\rho}_e) = \frac{\sigma_e^{\mathrm{m}}(\bar{\rho}_e)}{2} + \frac{\sqrt{\sigma_e^{\mathrm{m}}(\bar{\rho}_e)^2 + \gamma}}{2}. \quad (14)$$

This operation can be considered as a smooth $\max(\sigma_e^{\mathrm{m}}(\bar{\rho}_e), 0)$ operation, where γ is a small value making the function smooth around zero mean stress. This operation eliminates the effect of negative mean stresses in the modified Goodman correction which is given by:

$$\sigma_e^{\mathrm{a0}}(\bar{\rho}_e) = \sigma_e^{\mathrm{a}}(\bar{\rho}_e)\left(1 - \frac{\sigma_e^{\mathrm{m0}}(\bar{\rho}_e)}{\sigma_{\mathrm{U}}}\right)^{-1}, \quad (15)$$

where σ_{U} is the ultimate tensile strength of the material and $\sigma_e^{\mathrm{a0}}(\bar{\rho}_e)$ is the stress amplitude we want to constrain, which is valid for comparison with an SN-diagram.

The stress amplitude of the largest stress cycle is constrained with the fatigue limit of the material σ_{D} according to:

$$g_e^{\mathrm{f}} = \left(\frac{\sigma_e^{\mathrm{a0}}(\bar{\rho}_e)}{\sigma_{\mathrm{D}}} - 1\right)\bar{\rho}_e \le 0, \ e \in \Omega \quad (16)$$

The fatigue constraint g_e^{f} is multiplied with $\bar{\rho}_e$, as the constraint should not apply to void elements (vanishing constraints) and this multiplication ensures that the constraints are satisfied when an element is at zero density. The result is a large set of local constraints on the design domain. The large set of local constraints is problematic, as this significantly reduces the efficiency of the adjoint method used to compute the gradients. To solve this, the local constraints are aggregated into a single global constraint by estimating the maximum constraint value using the lower bound KS-function from Verbart et al. (2017) as follows:

$$g_{\mathrm{G}}^{\mathrm{f}} = \frac{1}{k_2} \ln\left(\frac{1}{V_\Omega} \sum_{e \in \Omega} e^{k_2 g_e^{\mathrm{f}}}\right). \quad (17)$$

Note that the upper bound KS-function was used for the maximum and minimum stress approximation and the lower bound KS-function for the constraint aggregation. The reason for this is that the KS-function is more accurate in estimating peak values in an array and the KS-mean more accurate when the values are at the same level (Holmberg et al., 2013). The assumption is that the former is better suited for approximating the max and min stress in time and the latter for aggregating the constraints. The aggregation parameters k_1 and k_2 are chosen as $k_1 = k_2 = 20$.

The global stress constraint $g_{\mathrm{G}}^{\mathrm{s}}$ is obtained following Equations 16 and 17, but in the equations $\sigma_e^{\mathrm{a0}}(\bar{\rho}_e)$, σ_{D} and g_e^{f} are replaced by the relaxed von Mises stress $\tilde{\sigma}_e^{\mathrm{vm}}(\bar{\rho}_e)$, yield stress σ_{Y} and the local stress constraints g_e^{s} respectively.

2.4. Combining cyclic symmetry and quasi-static analysis

For cyclic symmetric design problems which adhere to the conditions stated in Section 1.4, the cyclic symmetry and the quasi-static analysis can be combined in a clever way.
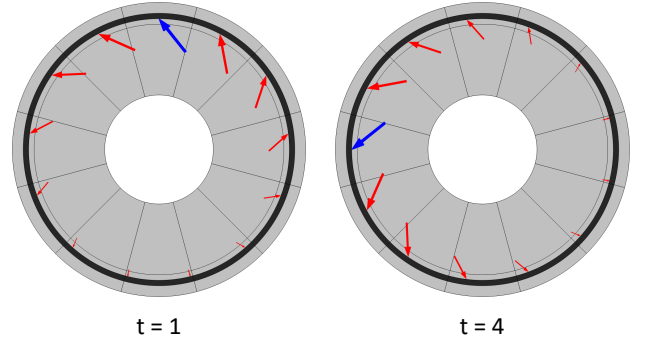

Figure 5: Two time steps of a cyclic symmetric problem with 12 segments and 13 loads. The loads move counterclockwise. Time step 4 is essentially the same as physically rotating time step 1 counterclockwise by three segment. The load with the largest magnitude is plotted in blue for both time steps to illustrate how the model appears to have rotated.

Cyclic symmetry is enforced by making material properties at corresponding locations dependent on the same design variable, which is similar to the method used by Kosaka and Swan (1999). A benefit to this approach is that the density filter can cross the boundary to neighboring segments, ensuring a smooth density transition between them. This enforced cyclic symmetry approach would normally not save computation time for the FE-analysis as the response of the entire structure is computed. However, for the type of design problems mentioned, the responses of the additional segments hold useful information for the quasi-static analysis. The problem shown in Figure 5 contains 13 equidistantly spaced point loads around the circumference of 12 segments. Together they appear to act like a single counterclockwise traveling wave. By looking at the difference between time steps 1 and 4 shown, it can be noted that this is the same as physically rotating the model three segment counterclockwise. For this problem, a *single* static FE-analysis of the entire cyclic symmetric structure, therefore, is a physical representation of a quasi-static analysis containing a number of time steps equal to the number of forces present. The disadvantage of having to compute the entire structural response when enforcing symmetry in the presented way is, therefore, negated. This is a key insight that is exploited in the proposed method.

It should be noted that depending on the number of segments and number of traveling waves, it could occur that the entire structure contains two or more identical sets of segments. The copies of a set of segments do not provide additional information for the quasi-static analysis and are therefore redundant. The copies can in such cases be removed from the analysis by applying a periodic boundary condition like was used by Barbarosie and Toader (2010). This results in a lower computation cost per time step but more time steps need to be evaluated for the quasi-static analysis, as the smaller set of segments return less time information. For further clarification if there would have been 14 equidistantly spaced loads over the 12 segments, there would be 6 unique segments. Segments that are opposite of each other are loaded identically. This unique

set of segments contains 7 loads and therefore provides 7 time steps. The number of identical sets can be determined from the largest common divider between the amount of segments and the amount of loads.

2.5. Optimization approach

Due to the large amount of design variables $\boldsymbol{\rho}$ used in TO, a gradient based optimization method is necessary to make the optimization problem computationally feasible. A sensitivity analysis is, therefore, performed after the FE-analysis to obtain the gradients of the constraints and objective function with respect to the design variables. The adjoint method (Michaleris et al., 1994) is used to compute the sensitivities, which is efficient for problems containing many design variables and few functional responses. The general expression of the gradient of a set of functionals $\mathbf{h}(\mathbf{u}(\boldsymbol{\rho}), \boldsymbol{\rho})$ is as follows:

$$\frac{\mathrm{d}h_i}{\mathrm{d}\rho_j} = \frac{\partial h_i}{\partial \rho_j} + \frac{\partial h_i}{\partial \mathbf{u}} \cdot \frac{\mathrm{d}\mathbf{u}}{\mathrm{d}\rho_j}, \tag{18}$$

where $\frac{\partial h_i}{\partial \rho_j}$ and $\frac{\partial h_i}{\partial \mathbf{u}}$ are explicit terms and $\frac{\mathrm{d}\mathbf{u}}{\mathrm{d}\rho_j}$ is an implicit term. The explicit terms can be worked out analytically, the implicit term on the other hand is computationally expensive. The adjoint method eliminates this term from the problem by augmenting the functional with the static equilibrium equations: $\mathbf{K}(\boldsymbol{\rho})\mathbf{u} - \mathbf{f} = 0$ with a Lagrange multiplier λ_i. This adds the following term to Equation 18: $+\lambda_i \left(\frac{\partial \mathbf{f}}{\partial \rho_j} - \frac{\partial \mathbf{K}}{\partial \rho_j}\mathbf{u} - \mathbf{K}\frac{\mathrm{d}\mathbf{u}}{\mathrm{d}\rho_j} \right)$. After rearranging the terms into explicit and implicit parts as follows:

$$\frac{dh_i}{d\rho_j} = \frac{\partial h_i}{\partial \rho_j} + \lambda_i \left(\frac{\partial \mathbf{f}}{\partial \rho_j} - \frac{\partial \mathbf{K}}{\partial \rho_j}\mathbf{u} \right) + \left(\frac{\partial h_i}{\partial \mathbf{u}} - \lambda_i\mathbf{K} \right) \frac{d\mathbf{u}}{d\rho_j}, \tag{19}$$

the implicit term $\frac{\mathrm{d}\mathbf{u}}{\mathrm{d}\rho_j}$ can be eliminated from the problem by computing the Lagrange multiplier such that $\frac{\partial h_i}{\partial \mathbf{u}} - \lambda_i\mathbf{K} = 0$.

The explicit terms $\frac{\partial h_i}{\partial \rho_j}$ and $\frac{\partial h_i}{\partial \mathbf{u}}$ have to be worked out analytically, which is shown for Equations 9, 10 & 11, as these

Table 1: Properties and settings

Property	Value
Young's modulus	$E_0 = 200\,[\text{GPa}]$
Lower bound Young's modulus	$E_{\min} = 10^{-9}E_0$
Poisson's ratio	$\nu = 0.3$
Yield stress	$\sigma_Y = 75\,[\text{MPa}]$
Ultimate tensile stress	$\sigma_U = 100\,[\text{MPa}]$
Endurance limit	$\sigma_D = 50\,[\text{MPa}]$
2D Model	Plane stress
Thickness	$10\,[\text{mm}]$
Element type	Bilinear quadrilateral
Element size	$1\,[\text{mm}]$
Filter radius	$R_{\text{PDE}} = 1.5\,[\text{mm}]$
Projection slope parameter	$\beta = 6$
Aggregation parameters	$k_1 = k_2 = 20$
SIMP parameter stiffness	$p = 3$
SIMP parameter stress	$q = 2.5$
Initial density distribution	$\boldsymbol{\rho} = \mathbf{1}$

are specific to the presented method of this paper. Sensitivities of the other steps of the method and the objective function can be found in their respective literature. The sensitivity of the maximum signed von Mises stress with respect to the design variables $\frac{\partial \sigma_e^{\max}(\bar{\rho}_e)}{\partial \rho_e}$ reads as follows:

$$\frac{\partial \sigma_e^{\max}(\bar{\rho}_e)}{\partial \rho_e} = \frac{\left(\sum_{i=1}^{N} e^{k_1\tilde{\sigma}_e(\bar{\rho}_e, t_i)} \frac{\partial \tilde{\sigma}_e(\bar{\rho}_e, t_i)}{\partial \rho_e} \right)}{\left(\sum_{i=1}^{N} e^{k_1\tilde{\sigma}_e(\bar{\rho}_e, t_i)} \right)}. \tag{20}$$

The sensitivity of the minimum signed von Mises stress $\frac{\partial \sigma_e^{\min}(\bar{\rho}_e)}{\partial \rho_e}$ is obtained by replacing k_1 with $-k_1$. The sensitivity of the signed von Mises stress $\frac{\partial \tilde{\sigma}_e(\bar{\rho}_e, t_i)}{\partial \rho_e}$ is as follows:

$$\frac{\partial \tilde{\sigma}_e(\bar{\rho}_e, t_i)}{\partial \rho_e} = \tanh(\sigma_e^{\text{H}}(t_i)) \frac{\partial \tilde{\sigma}_e^{\text{vm}}(\bar{\rho}_e, t_i)}{\partial \rho_e}$$
$$+ \left(1 - \tanh^2(\sigma_e^{\text{H}}(t_i)) \right) \frac{\partial \sigma_e^{\text{H}}(t_i)}{\rho_e} \tilde{\sigma}_e^{\text{vm}}(\bar{\rho}_e, t_i), \tag{21}$$

where $\tilde{\sigma}_e^{\text{vm}}(\bar{\rho}_e, t_i) = \sqrt{3\mathbf{J}_2(\hat{\sigma}_e(\bar{\rho}_e, t_i))}$ is the von Mises stress. The sensitivities with respect to $\mathbf{u}$ are obtained equivalently.

The gradient based optimization algorithm used is GCMMA (Globally Convergent Method of Moving Asymptotes) (Svanberg, 2002), which is an extension to the commonly used Method of Moving Asymptotes (MMA) by Svanberg (1987). The ordinary MMA solves the optimization problem by first approximating a set of convex subproblems between two asymptotes at the current iteration. The asymptotes are updated based on information from the previous iteration, while the convex approximations are based on the gradient information at the current iteration. The set of convex subproblems can be efficiently solved using a dual method and the optimal solution found are the new design variable values $\boldsymbol{\rho}$ for the next iteration. GCMMA extends MMA by considering inner and outer iterations. The outer iterations represent the regular MMA. However, for every outer iteration, there can be multiple inner iterations. The GCMMA method aims to always reduce the objective function between outer iterations using these inner iterations.

For the examples considered in this paper the default settings are used with the addition of a move limit of 0.1. The maximum number of inner iteration per outer iterations is set to 10. The outer iterations continue until either the optimality tolerance at 0.001 is obtained, which is the default convergence criteria of GCMMA in COMSOL, or a maximum outer iteration of 500 is reached.

3. Test problems and procedures

The method is implemented in COMSOL Multiphysics using the structural mechanics and optimization modules. Unless specified otherwise, the properties and settings as listed in Table 1 are used for the test problems analysed. The test problems contain both 2D and 3D problems. For the first three problems, which are 2D, cyclic symmetry is not yet considered. The intend of these first three problems is to test the performance of the non-proportional fatigue constraint method

independently. Thereafter, the method is applied to two cyclic symmetric problems, the first of which is in 2D and the second in 3D.

3.1. Fatigue test problems

The three Test problems considered for the independent fatigue constraint test are: an L-bracket subjected to a proportional periodic load (Figure 6), an L-bracket subjected to two periodic out-of-phase loads (Figure 7) and a beam subjected to a time varying moving load (Figure 8). For each test case two optimization approaches are considered, one proportional and the other non-proportional.

For the proportional approach assumptions are made to replace non-proportional loading by a proportional interpretation of the loading if necessary. In the proportional optimization approach Equations (10) and (11) are removed and σ_e^{max} and σ_e^{min} are instead obtained from scaling a reference stress field, as obtained from a unit load, with the known maximum and minimum force in time.

For the non-proportional optimization approach no simplifications of the loading are necessary and the method as described in Section 2.3 is used. The results of both approaches are compared to establish to what extent using the more computationally intensive non-proportional method improves the constraint adherence of the optimised design as opposed to making proportional assumptions. It is expected that the proportional approach will show a significantly worse fatigue performance than the non-proportional approach for the problems subjected to non-proportional loading when the non simplified loading is applied to the optimized geometry.

3.1.1. L-bracket with proportional periodic loading

The L-bracket is a commonly considered design problem for stress and fatigue based optimization problems, due to the stress concentration at the re-entrant corner. For this first Test problem, a proportional sinusoidal load case is considered with a mean load F_m = 0.25 [kN] and load amplitude F_a = 1 [kN]. Since the load case is proportional, both the proportional and non-proportional approach should yield acceptable results. The main intend of this problem is, therefore, to establish a benchmark to which the problems subjected to non-proportional loading can be compared.

The design problem is shown in Figure 6 and the properties and settings used are listed in Table 1. The proportional load is distributed and applied over 7 nodes at the top of the right most boundary and a small section of 4 x 6 elements is excluded from the design domain, meaning that the density is set to fully solid and local constraints are not included in the constraint aggregation. This is to avoid large local stresses at the application point from influencing the global constraint. Along the inside boundaries, connected to the re-entrant corner, a passive void region is added which allows the filter to create a smooth transition between void and solid around the re-entrant corner.
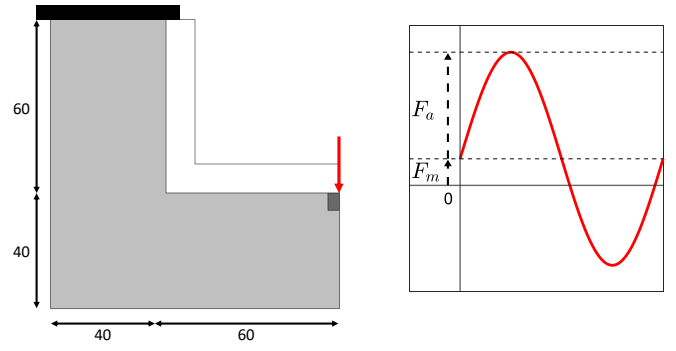

Figure 6: Test problem 1 is an L-bracket. The design domain is shown in light gray. The bracket is fixed at the black bar and a small region around the load application point marked in dark gray is excluded from the design domain. The proportional load is sinusoidal with an amplitude F_a = 1 [kN] and a mean F_m = 0.25 [kN]. Dimensions are in [mm].

3.1.2. L-bracket with non-proportional out-of-phase loading

In the second problem a non-proportional load case is applied to the L-bracket. Apart from the load case the problem is equivalent to the first test problem. The loading consists of two proportional sinusoidal loads P1 and P2 in x and y direction at the application point. Both loads have an amplitude of 1 [kN] and a mean of 0 [kN]. The loads are out-of-phase with respect to each other by a phase of 90°, which makes the combined loading non-proportional. The resulting load case is a load that has a constant magnitude of 1 [kN] and rotates with a constant rotation speed around the application point as illustrated in Figure 7.

For the proportional approach the proportional loads P1 and P2 are evaluated for fatigue separately from each other and are combined in the optimization by implementing them as a multiple loading optimization. In the non-proportional approach 12 time steps are used in the quasi-static analysis for one full rotation of the load.
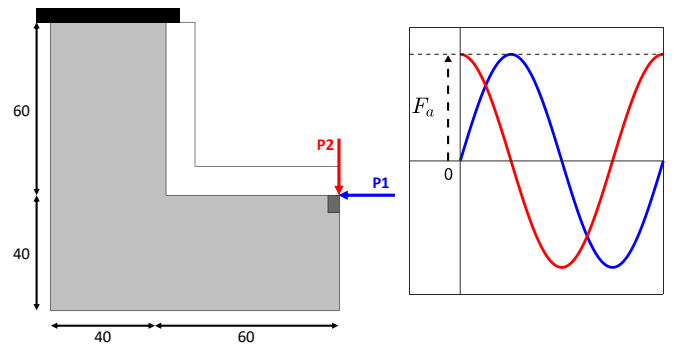

Figure 7: Test problem 2 is the same L-bracket from Test problem 1, but now a horizontal (P1) and vertical (P2) load are applied both with an amplitude F_a = 1 [kN] and a mean F_m = 0.25 [kN]. The loads are 90° out of phase, which results in a rotating load with constant rotation speed and a constant magnitude of 1 [kN]. Dimensions are in [mm].

3.1.3. Moving load across beam

For the third fatigue test problem a moving load across a beam is considered. The design problem is shown in Figure 8 and the properties and settings used are listed in Table 1. A load moves along the top surface of the beam at a constant speed and is equally distributed over 11 nodes. The magnitude of the load varies sinusoidal with respect to its position on the beam with a mean of 2.5 [kN] and an amplitude of 1.5 [kN]. The beam has roller connections at both lower ends. The top layer is a passive region set to full solid, but is included in the constraint aggregation, as the load is distributed over a sufficient amount of nodes to avoid too high application stresses.

A proportional interpretation of the loading is made by defining a proportional load case at critical time points of the moving load. At the locations of these critical time points a proportional load is applied. This proportional load has a maximum equal to the magnitude of the moving load at that time point and a minimum equal to 0 [kN], which represents the presence and absence of the moving load at that location.

Similar to the proportional approach of the second test problem these load cases are evaluated for fatigue separately from each other and combined in the optimization by implementing them as a multiple loading optimization. For this problem three critical time steps where the moving load magnitude is at its peak are identified, which conveniently cover the range of motion as well. For the quasi-static analysis performed in the non-proportional approach 13 time steps are used.

3.2. Cyclic symmetric fatigue problems

The remaining two problems analysed are cyclic symmetric, which is exploited to reduce the computation cost. The first problem considered is a 2D ring with flanges subjected to time-varying moving loads (Figure 10). The second problem is a 3D casing where time-varying moving loads travel along the inside boundary (Figure 11.

Figure 8: Test problem 3 is a beam with a moving load that varies sinusoidal between 1 [kN] and 4 [kN] with respect to its position on the beam. The light gray region is the design domain. The dark gray bar is set to solid material and the blue boundary connections are rolling contacts. Dimensions are in [mm].
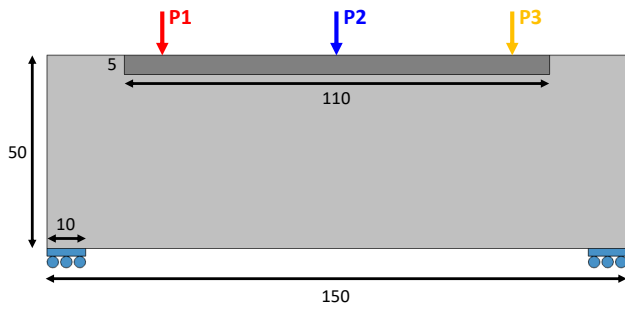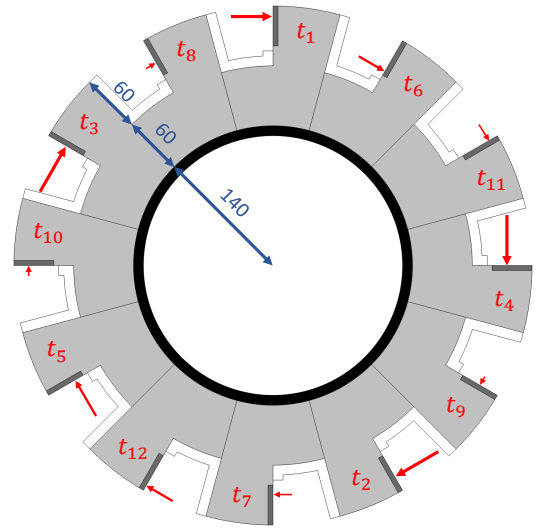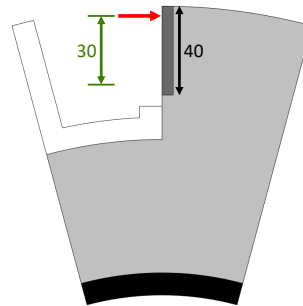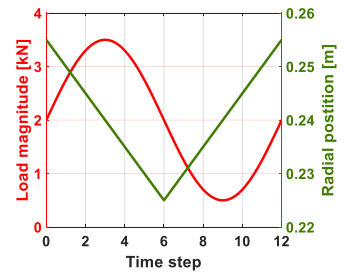

Figure 9: The proportional interpretation of Test problem 3 is three separate proportional load cases P1, P2, and P3 with a maximum magnitude of 4 [kN] and a minimum of 0 [kN]. The separate load cases are evaluated for fatigue independently and combined in a multiple loading optimization.

(a) Total problem showing the represented time steps by the segments.

(b) A single segment

(c) Magnitude and position of the moving load over one period.

Figure 10: Test problem 4 is the first cyclic symmetric problem considered. It consits of 12 segments each containing a radially moving load. The inner ring (black) is fixed. The dark gray region is solid material and excluded from the design domain (light gray). Along the boundaries connected to the re-entrance corners is a passive void region. Dimensions are in [mm].

3.2.1. Cyclic symmetric problem in 2D

The first cyclic symmetric problem, shown in Figure 10, consist of 12 identical segments. It is fixed at the inner ring. The boundary loads move with a constant speed back and forth in the radial direction. The loads are applied over 6 nodes and magnitudes vary sinusoidal with a mean of 2 [kN] and amplitude of 1.5 [kN], as shown in Figure 10c. The design domain (one segment) is meshed using 26 354 triangular mesh elements and is copied to the other eleven segments. The density distribution of the design domain is mapped onto the other segments to enforce the cyclic symmetry. The constant shift in time between the segments is 5 time steps clockwise or equivalently 7 time steps counterclockwise, as illustrated in Figure 10a. For this setup each segment provides a unique time step for the quasi-static analysis. Therefore, a single static response of the whole structure returns 12 time steps, which is considered sufficient to describe the load case.

3.2.2. Cyclic symmetric problem in 3D

The second cyclic symmetric problem analysed is 3-dimensional, as shown in Figure 11. It consists of 12 cyclic symmetric segments. Each segment has an identical mesh containing 47 498 tetrahedral elements with an average element size of 25 [mm], giving a total mesh of 569 976 elements. Since this mesh is relatively coarse with respect to the dimensions of the problem, a smaller filter radius of $R_{\text{PDE}} = 1\,l_e$, giving $R_{\text{PDE}} = 25$ [mm], is used to allow for smaller features. 13 loads are equidistantly spaced around the diameter, as shown in Figure 12. The loads move in tangential direction and cross between segments. Both the radial and tangential components of the load magnitudes vary in time according to the graph shown in Figure 13. The constant shift in time between the segments is 1 time step both clockwise as counterclockwise. Each load represents a time step in the quasi static analysis. As there are 13 loads distributed over 12 segments, there is a segment containing two of the loads. This segment represents the time steps for both these loads and the static response of the complete structure, therefore, provides 13 time steps for the quasi-static analysis, which is considered sufficient for this problem.

3.3. Fatigue validation

The results of both proportional and non-proportional approaches are validated for fatigue failure by applying the non-simplified loading to the optimized structure. To define a geometry from the optimized result, the density distribution is first projected on a twice as fine mesh using a density filter step to improve the smoothness of transitions between material and void. COMSOL projects mesh data like the density distribution as a continuous field using shape functions. A geometry is extracted by defining the boundaries at $\bar{\rho} = 0.5$. Densities above are set to full material and densities below to void. The resulting geometry is meshed with linear triangular elements for the 2D Test problems and linear tetrahedral elements for the 3D Test problem using a twice as fine mesh size as was used for the optimization.
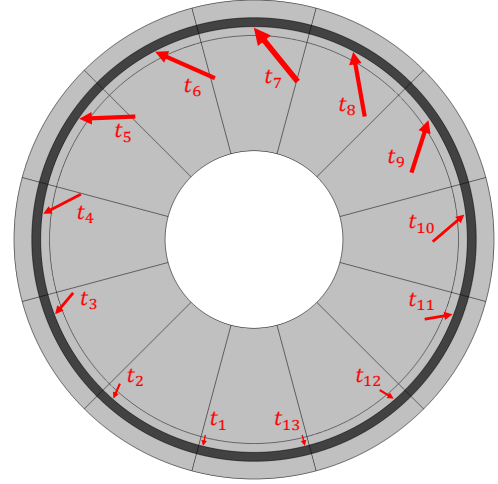

Figure 11: Test problem 5 consists of 12 cyclic symmetric segments in 3D. The time steps for the 13 equidistantly spaced loads are shown.
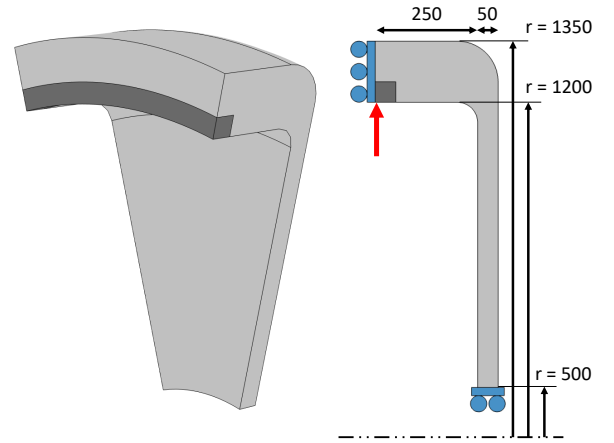

Figure 12: The dimensions and boundary conditions of Test problem 5. The dark gray ring where the load is applied is solid material and is excluded from the design domain. The blue boundaries are roller connections. Dimensions are in [mm].
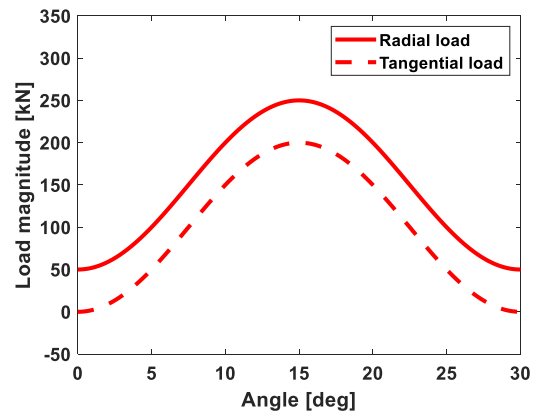

Figure 13: The magnitude of the loads in Test problem 5 expressed in radial and tangential directions with respect to the angular coordinate of a segment.

11

A quasi-static FE-analysis is performed and material fatigue is determined by evaluating the largest variation in the signed von Mises stress, which is the same approach used in Section 2.3. The fatigue constraint is evaluated in at least 10 000 evenly distributed points, which are used to establish percentually how much of the geometry domain adheres to the constraint. Furthermore, for the sampled evaluation points, the stress amplitude is plotted with respect to the mean stress in a plot as shown in Figure 4. This shows local adherence to the fatigue and yield stress constraints defined by the failure envelope.

In addition to the variation in signed von Mises stress, the Dang Van critical plane method Karolczuk et al. (2016) has been used to evaluate fatigue, as this is regarded as a more accurate fatigue approximation method for non-proportional loading (Papuga et al., 2012). The validation using the signed von Mises stress is shown in Section 4.1 & 4.2 together with the optimized density distribution, whereas the results of the Dang Van method are discussed separately in Section 4.4 and compared to those of the signed von Mises criterion.

4. Results & Discussion

In this section the results of the Test problems described in the previous section are presented and discussed. First the three fatigue test problems and thereafter the 2D and 3D cyclic symmetric problems. Ultimately, the validations using a critical plane method are shown and compared to the signed von mises stress validation.

4.1. Fatigue test results

For each fatigue test problem two optimization approaches were performed, a proportional approach and a non-proportional approach. The results for both are presented and compared.

4.1.1. Test problem 1: L-bracket with proportional periodic loading

The results for both problem definitions were obtained after 500 iterations and are shown in Figure 15 and Table 2. As expected, the results for both approaches are very similar and nearly indistinguishable. The proportional approach has a material usage of 0.3151, which is about 0.6% lower than the 0.3169 of the non-proportional approach. However, the percentage of the domain which satisfies the fatigue constraint is slightly worse for the proportional method at 97.1% versus the 97.5% of the non-proportional approach.

The difference in volume usage and constraint adherence between both approaches can be explained by the fact that the non-proportional approach makes an overestimation in its approximation of the largest stress cycle. This makes the approach more conservative and results in the trade off in volume performance and constraint performance.

Both approaches show a maximum normalized fatigue stress peak $\frac{\sigma_e^{a0}}{\sigma_D}$ that is significantly higher that allowable. A peak of 1.3922 for the proportional approach and a peak
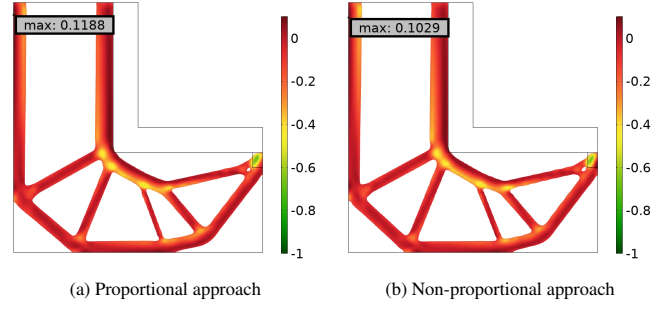

(a) Proportional approach   (b) Non-proportional approach

Figure 14: The local fatigue constraint values g_e^{f}, which are aggregated using the lower bound KS-function. Results are shown for $\rho \leq 0.5$.

of 1.3507 for the non-proportional approach. There are a couple of accountable reasons that contribute to these peaks. To start, from Figure 14 can be seen that the lower bound aggregation function underestimates the true local maximum constraint violation by about 10%. Secondly, due to the SIMP interpolation of the material properties, which was necessary to enforce the optimization towards a solid and void material distribution, representation of stresses by intermediate density variables found in the transition boundary is less accurate. When the sharpness of the boundary increases, as was done in the validation, the stresses increase. At last the large peaks can to an extent be attributed to the way the final result is interpreted at the 0.5 density threshold for the validation, as explained in Section 3.3. Due to the underlying rectangular mesh, the threshold gives a boundary that is not perfectly smooth. This results in local stress peaks and, therefore, larger stress cycles.

In Appendix A a manual design iteration is performed in an attempt to reduce local stress peaks which can be explained from this phenomenon by improving the smoothness of boundaries while avoiding adding significant extra volume. After the manual iteration the maximum normalized fatigue stress are about 1.24 for the proportional approach and 1.19 for the non-proportional approach. This is considerably less while only increasing the volume by 0.5% and 0.7% respectively, which shows that the interpretation of a geometry from the optimized result is a significant reason for these higher then expected fatigue stresses found. Due to the manual iteration being inconsistent, the maximum constraint violation is not taken as a measure of comparison for the remaining Test problems but the domain percentages shown in Table 2 are instead.

The local stress behaviours are plotted in Figure 15c & 15d. Two straight lines are apparent. This is expected for proportional loading. The steepness of the lines can be derived from the choice of relative magnitude between the amplitude and mean of the proportional load. Convergence of the objective functions is shown in Figure 18a & 18d. The convergence of both approaches is smooth and similar.

4.1.2. Test problem 2: L-bracket with non-proportional out-of-phase loading

The results for both problem definitions were obtained after 500 iterations and are shown in Figure 16 and Table 3. The

12

Table 2: Results of Test problem 1: the normalised material usage V and local fatigue constraint adherence differentiated into five ranges from satisfied (≤ 1) to exceeded by a factor larger than 1.2 are shown for the proportional (P) and non-proportional approach (NP). The fatigue constraint adherence is shown for both the optimization model as well as the validation model.

Test problem 1	V	≤ 1	$1 - 1.05$	$1.05 - 1.10$	$1.10 - 1.20$	> 1.20
P validation result	0.3151	97.1%	2.1%	0.5%	0.3%	0.1%
NP validation result	0.3169	97.5%	1.9%	0.3%	0.2%	$< 0.1\%$

(a) Proportional approach

(b) Non-proportional approach
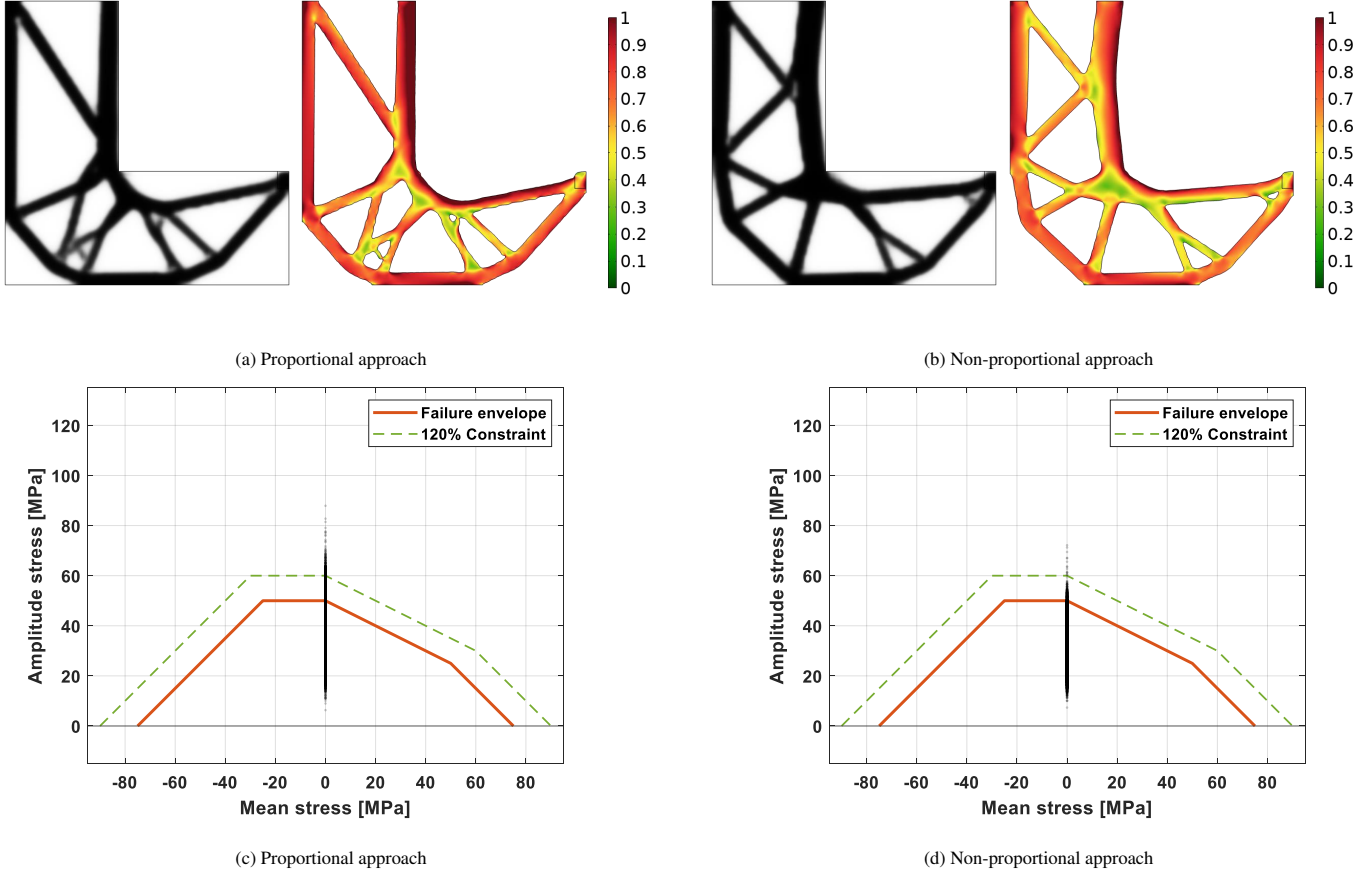
(c) Proportional approach

(d) Non-proportional approach
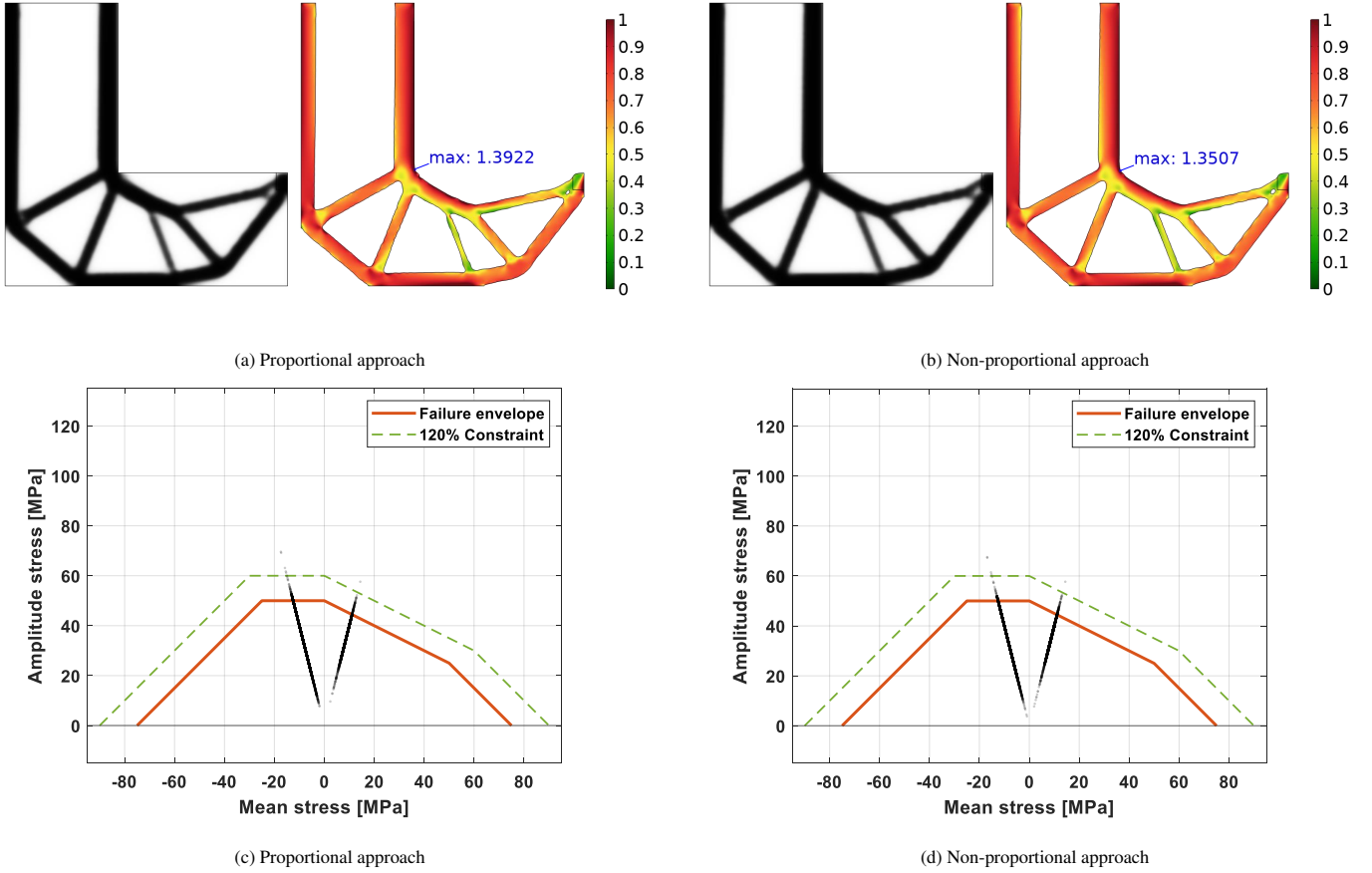
Figure 15: Results of Test problem 1. (a) and (b) show the density distribution and the normalized fatigue stress amplitude $\frac{\sigma_e^{a0}}{\sigma_D}$. (c) and (d) show a scatter plot of the local stress behaviour.

density distribution shows a clear difference in topology. The proportional approach has a material usage of 0.3606, which is about 9.3% lower than the 0.4010 of the non-proportional approach. As expected, however, the percentage of the domain which satisfies the fatigue constraint is significantly worse for the proportional method at 90.3% versus the 97.8% of the non-proportional approach which is in accordance to the results from Test problem 1. Convergence of the objective functions is plotted in Figure 18b & 18e, which is again smooth and similar.

The difference in material usage and constraint adherence between both approaches can be explained by the fact that the proportional method only considers loads in the horizontal and vertical direction separately and therefore does not account for diagonal loads, which results in too high stresses when the rotating load is not oriented horizontally or vertically. The non-

proportional approach does consider the different orientations of the load and is therefore able to properly constrain the load and achieve results that are on accordance to the results of Test problem 1. To properly constrain the load more material usage is required. The result of the proportional definition could arguably be improved by increasing the number of loads with different orientations used in the multiple loading optimization.

Looking at the local stress behaviour in Figure 16c & 16d, again a straight line is observed even though the loading is non-proportional. In this specific case the straight line is obtained from the fact that for every load, a counter load points in the opposite direction at some time during the rotation. This results into no present mean stress of the largest stress cycle in the structure after one rotation. Taking this into consideration, the results of the proportional definition might yield a comparable

13

Table 3: Results of Test problem 2: the normalised material usage V and local fatigue constraint adherence differentiated into five ranges from satisfied (≤ 1) to exceeded by a factor larger than 1.2 are shown for the proportional (P) and non-proportional approach (NP).

Test problem 2	V	≤ 1	$1 - 1.05$	$1.05 - 1.10$	$1.10 - 1.20$	> 1.20
P validation result	0.3606	90.3%	2.7%	2.1%	2.8%	2.1%
NP validation result	0.4010	97.8%	1.3%	0.7%	0.2%	0.1%

(a) Proportional approach

(b) Non-proportional approach
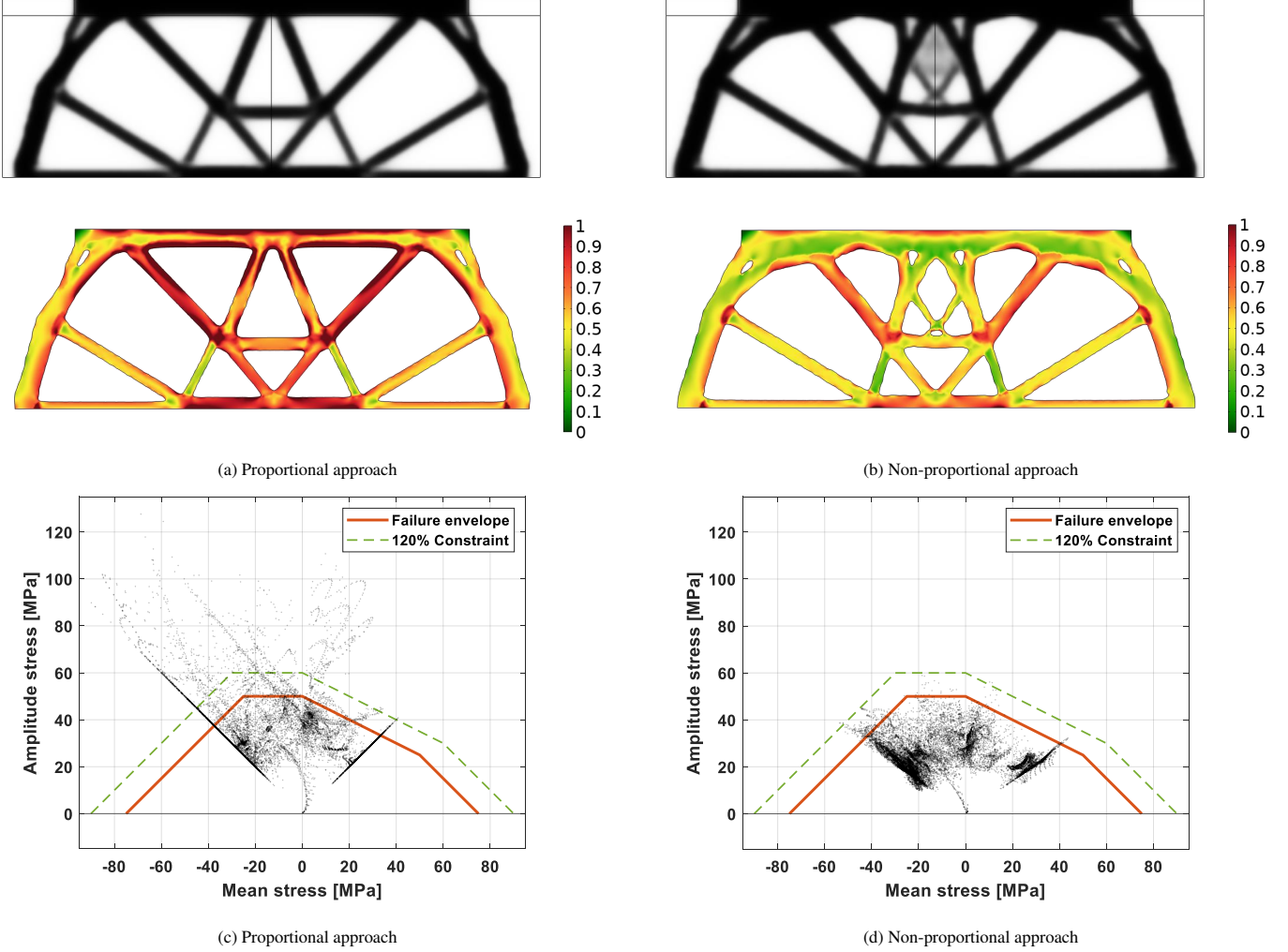

(c) Proportional approach

(d) Non-proportional approach

Figure 16: Results of Test problem 2: (a) and (b) show the density distribution and normalized fatigue stress amplitude $\frac{\sigma_e^{a0}}{\sigma_D}$. (c) and (d) show a scatter plot of the local stress behaviour

result when more load cases are used.

4.1.3. Test problem 3: Moving load across beam

The results of both problem definitions are shown in Figure 17 and Table 4. Smooth convergence of the objective functions is shown in Figure 18c & 18f. The proportional problem reached the maximum number of 500 iterations, whereas the non-proportional problem reached the convergence criteria after 460 iterations.

A slight difference in topology can be observed between the two approaches. The main difference is close to the boundary where the loading is applied. With a material usage of 0.2879, which is about 20.3% lower than 0.3556, similar to the previously analysed problem the proportional approach shows a lower material usage than the non-proportional approach, but at 86.6% performs significantly worse in adhering to the

fatigue constraint opposed to the 99.7% of the non-proportional approach.

The local stress behaviour in Figure 17c & 17d shows that the violation of constraints is quite significant for the proportional simplification of the design problem. Nevertheless, it did manage to obtain the main topological features found in the non-simplified problem. This shows that simplified problems, where choosing the critical time steps is quite intuitive, might still result in an acceptable initial design, but quite some post processing will be necessary to satisfy the constraints. In general a proportional simplification might not be trivial and making drastic assumptions about the loading could be undesirable.

An observation, which was made for moving load problems, is that the method struggled to fully converge to an all black and white density distribution and a gray region remains in the

14

Table 4: Results of Test problem 3: the normalised material usage V and local fatigue constraint adherence differentiated into five ranges from satisfied (≤ 1) to exceeded by a factor larger than 1.2 are shown for the proportional (P) and non-proportional approach (NP).

Test problem 3	V	≤ 1	$1 - 1.05$	$1.05 - 1.10$	$1.10 - 1.20$	> 1.20
P validation result	0.2879	86.6%	2.1%	1.8%	2.9%	6.5%
NP validation result	0.3556	99.7%	0.1%	0.1%	0.1%	< 0.1%

(a) Proportional approach

(b) Non-proportional approach

(c) Proportional approach

(d) Non-proportional approach

Figure 17: Results of Test problem 3: (a) and (b) show the density distribution and normalized fatigue stress amplitude $\frac{\sigma_e^{a0}}{\sigma_D}$. (c) and (d) show a scatter plot of the local stress behaviour

final result. This can also be observed at the top middle of Figure 17b. A definitive cause for this issue was not established. A possible explanation could be that the moving load can be seen as a distributed load over the entire range of motion. This issue of gray areas has been observed in existing research that considers distributed loads (Zhao and Wang, 2014).

4.2. Cyclic symmetric fatigue test results

For the cyclic symmetric problems only the non-proportional method has been considered.

4.2.1. Test problem 4: Cyclic symmetric problem in 2D

The optimization converged after 286 iterations and the results are shown in Figure 19 and Table 5. The resulting topology contains no major gray regions and has a final volume usage fraction of 0.2832. The local fatigue constraints are satisfied for 97.2% of the design domain. For the remaining 2.8%, where the constraint is violated, a comparable trend as in Test problem 1 can be observed, where the violations up to about 1.20 times the constraint can be attributed to the approximation of the aggregation function and the violations above 1.20 are mainly attributed to non-smooth boundaries of the optimized geometry.

From the local stress behaviour in Figure 19d can be

(a) Test problem 1: Proportional

(b) Test problem 2: Proportional

(c) Test problem 3: Proportional

(d) Test problem 1: Non-proportional

(e) Test problem 2: Non-proportional
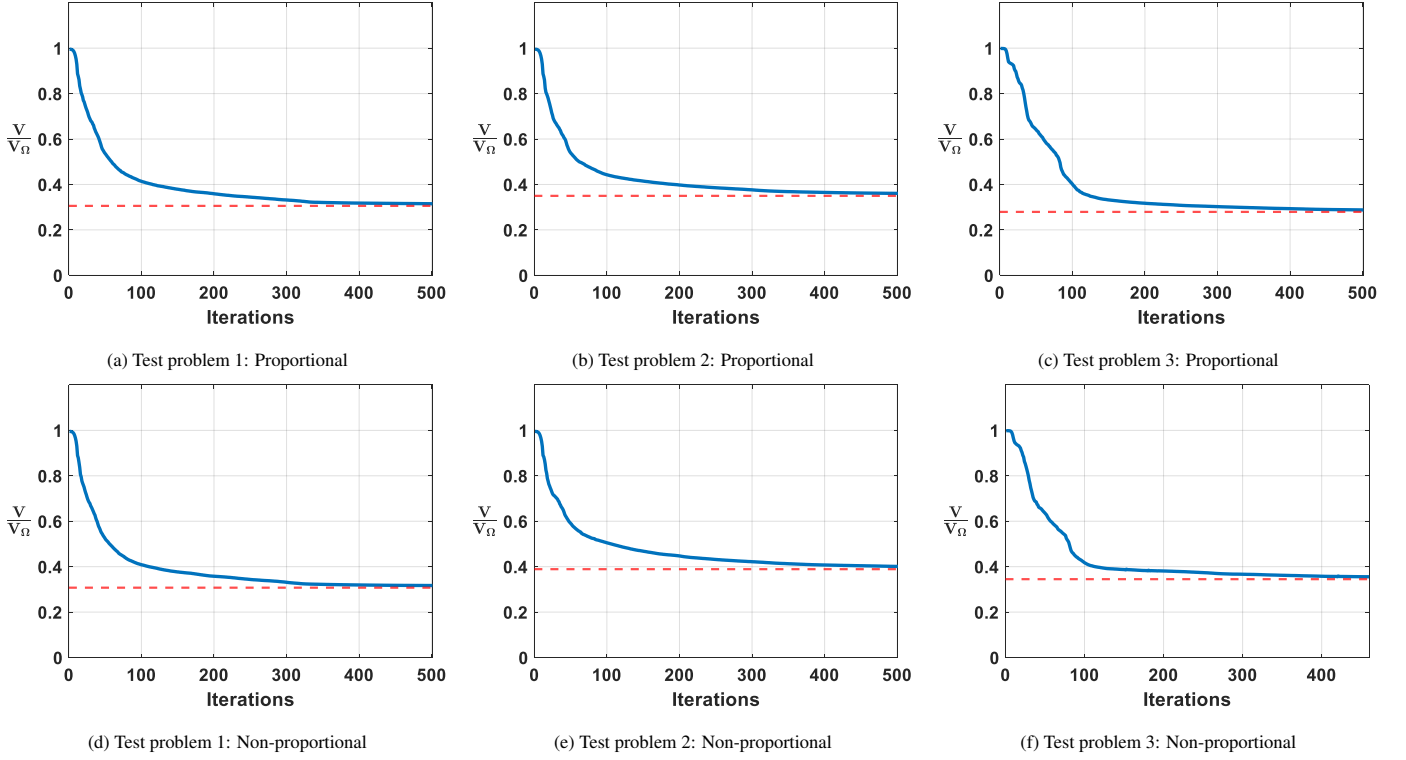
(f) Test problem 3: Non-proportional

Figure 18: Convergence of the objective function for Test problems 1, 2 and 3

observed that a large portion of the points cluster into two opposing lines. These points are most likely located at the two main truss features of the resulting topology, where the effect of the motion of the loads is not as significant. From the perspective of these points, the motion and magnitude variation of the load approaches proportional behaviour. The region where both trusses join at the inner ring seems to be a critical point. The reason for this is that a large tensile stress transverses through this region when the segment is under peak loading, while a large compressive stress transverses through this region when the neighbouring segment is under peak loading. This results in a large change in the signed von Mises stress. The signed von Mises stress is known to be less accurate for such regions and gives exaggerated stress cycles (Papuga et al., 2012). A further analysis of these regions using a critical plane fatigue method is discussed in Section 4.4.

4.2.2. Test problem 5: Cyclic symmetric problem in 3D

The results of the optimization are shown in Figure 20 and Table 6. The design converged to a black and white design in 96 iterations to a material usage factor of 0.4844. The local fatigue constraint adherence of 99.3% of the domain is in agreement with the results found in the previous analysed Test problems. From Figure 20d it can be seen that the local stress behaviour is widely distributed below the failure envelope. A proportional approach would most likely not have yielded a satisfactory result.

4.3. Discussion

It could be argued that the effectiveness of the presented method is not yet optimal, as the optimised topology might still need manual design iterations to fully eliminate the > 1.00 constraint violations. Some approaches are suggested to further improve the effectiveness of the method.

The first and simplest suggestion is to choose a more conservative fatigue constraint. The approximation error of the aggregation function for instance can be accounted for in the initial choice of the fatigue limit. A more conservative choice should significantly improve the local constraint adherence.

The second suggestion is a less heuristic approach. The global constraint scaling method introduced by Le et al. (2010) can be implemented, which scales the aggregated approximation based on the true and approximated maximum of the previous iteration and has been shown to work for stress based optimization problems. Applying constraint scaling during the optimisation is, however, not straightforward in the COMSOL environment.

A third suggestion is to replace the lower bound KS-function used in Equation 17 with the upper bound KS-function which is also used in Equations 10 & 11. This results in an overestimation of the local constraints instead of an underestimation. The choice between upper and lower bound KS-function, however, should be carefully considered depending on the design problem and the expected outcome, as the accuracy of the estimation is highly dependent on the distribution range of the aggregated data. For the Test problems considered in this paper, where only a fatigue/stress constraint

16

Table 5: Results of Test problem 4: the normalised material usage V and local fatigue constraint adherence differentiated into five ranges from satisfied (≤ 1) to exceeded by a factor larger than 1.2 are shown for non-proportional approach (NP).
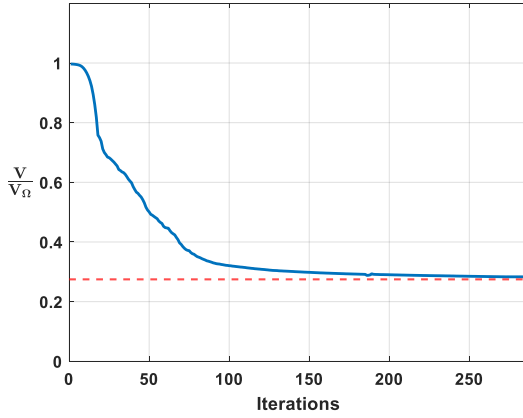
Test problem 4	V	≤ 1	$1 - 1.05$	$1.05 - 1.10$	$1.10 - 1.20$	> 1.20
NP validation result	0.2832	97.2%	1.5%	1.0%	0.3%	< 0.1%
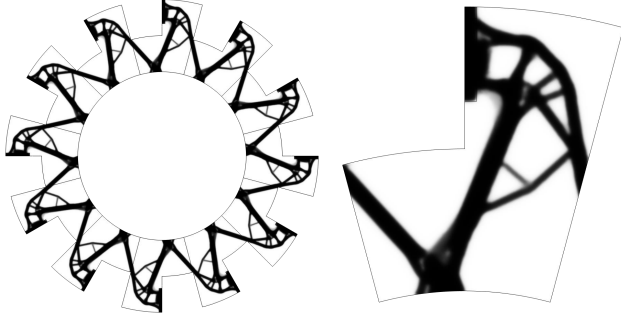
(a) Density distribution
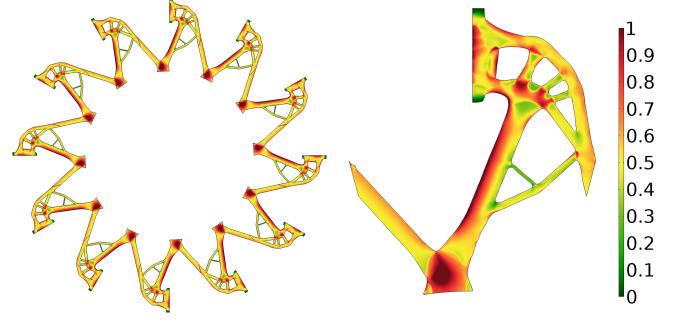
(b) Normalised fatigue stress

(c) Convergence of the objective function
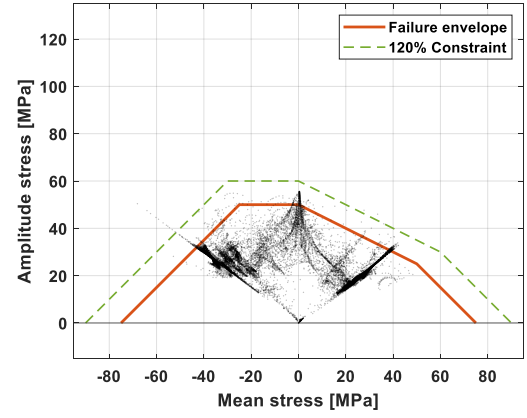
(d) Failure envelope of the local constraints

Figure 19: Results of Test problem 4: (a) and (b) show the density distribution and normalized fatigue stress amplitude $\frac{\sigma_e^{a0}}{\sigma_D}$. (c) and (d) show the objective function convergence and a scatter plot of the local stress behaviour.

is used, the upper bound might yield unnecessary conservative results, as a fully stressed final design is expected where the fatigue limit is approached throughout the geometry.

A last suggestion is to use the Augmented Lagrangian method to handle the local constraints as opposed to a global constraint method, which has been shown to have an improved local control (da Silva et al., 2021a).

A final observation, which was made while working out the discussed problems, is that Equation 15 contains a discontinuity. When $\sigma_e^{m0}(\bar{\rho}_e)$ approaches σ_U, then $\sigma_e^a(\bar{\rho}_e)$ is divided by zero and $\sigma_e^{a0}(\bar{\rho}_e)$ goes to infinity. For $\sigma_e^{m0}(\bar{\rho}_e) > \sigma_U$ the resulting stress amplitude even becomes negative which always fulfills the constraint. In practice the discontinuity does not necessarily cause problems during the optimization, since the additional stress constraint avoids $\sigma_e^{m0}(\bar{\rho}_e)$ from reaching σ_U. For the initial conditions it should definitely be avoided

though. A suggestion to avoid this issue is to implement a smooth $\min(\sigma_e^{m0}(\bar{\rho}_e), \sigma_U)$ operator (Jeong et al., 2015) after Equation 14, such that the mean stress cannot exceed the ultimate tensile stress. To further limit $\sigma_e^{a0}(\bar{\rho}_e)$ from becoming excessively large, Equation 15 can be modified as follows:

$$\sigma_e^{a0}(\bar{\rho}_e) = \sigma_e^a(\bar{\rho}_e)\left((1+\gamma) - \frac{\min(\sigma_e^{m0}(\bar{\rho}_e), \sigma_U)}{\sigma_U}\right)^{-1}. \quad (22)$$

The small offset γ limits the effect of a large compressive mean stress.

4.4. Critical plane method fatigue validation

Critical plane methods are considered to be more accurate for multiaxial fatigue evaluation of non-proportional loading

Table 6: Results of Test problem 5: the normalised material usage V and local fatigue constraint adherence differentiated into five ranges from satisfied (≤ 1) to exceeded by a factor larger than 1.2 are shown for non-proportional approach (NP).

Test problem 5	V	≤ 1	$1 - 1.05$	$1.05 - 1.10$	$1.10 - 1.20$	> 1.20
NP validation result	0.4844	99.3%	0.3%	0.1%	0.2%	0.2%
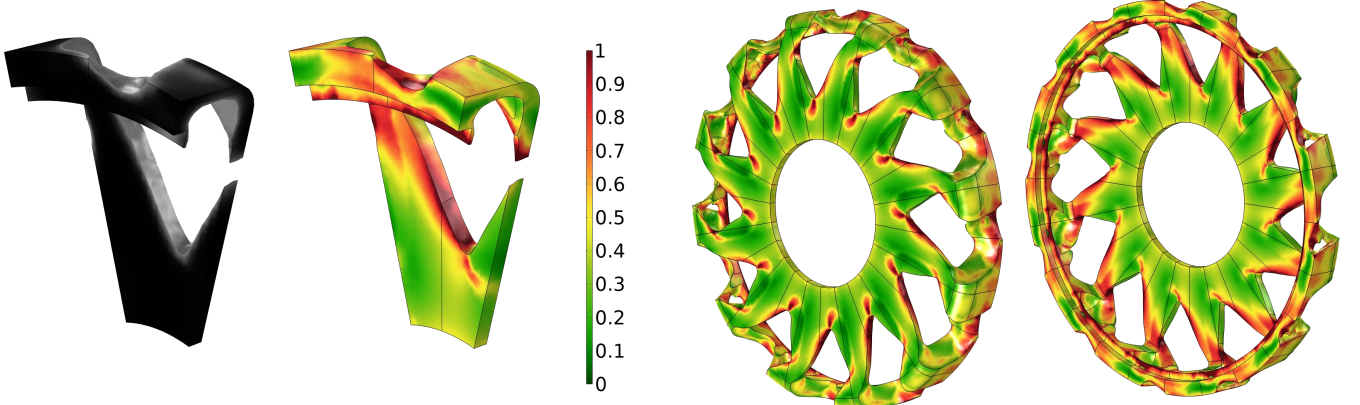
(a) Density distribution and normalised fatigue stress of the design domain

(b) Normalised fatigue stress of the full structure
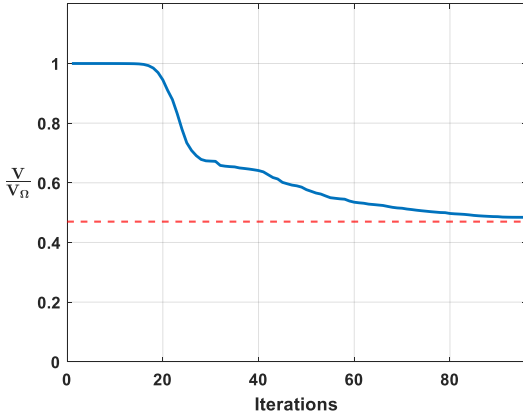
(c) Convergence of the objective function
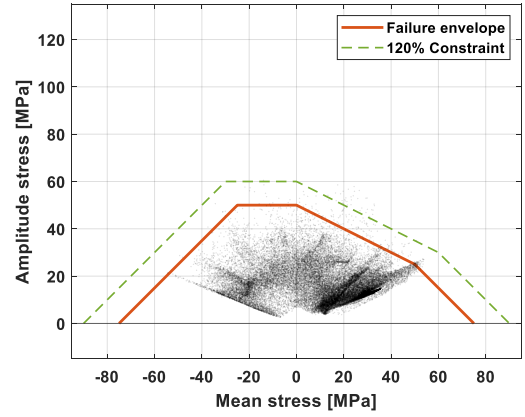
(d) Failure envelope of the local stress behaviour

Figure 20: Results of Test problem 5: (a) and (b) show the density distribution and normalized fatigue stress amplitude $\frac{\sigma_e^{a0}}{\sigma_D}$. show the objective function convergence and a scatter plot of the local stress behaviour.

(Carpinteri et al., 2017). The methods are based on locally defining the orientation of a failure plane, where some fatigue expression of stress or strain is maximal. The fatigue expression depends on the critical plane model used. The results obtained above using the non-proportional method are validated using the Dang Van critical plane method (Karolczuk et al., 2016) and compared to the results of the Signed von Mises stress fatigue evaluation shown in the previous subsections. The Dang Van method defines the fatigue expression as a combination of the shear stress $\tau_n(t)$ and the hydrostatic stress $\sigma^H(t)$. The orientation $\boldsymbol{n}$ of the critical plane is the plane of maximal shear

stress in time t according to:

$$\tau_D = \max_t (\max_{\boldsymbol{n}} (\tau_{\boldsymbol{n}}(t)) + \alpha \sigma^H(t)), \tag{23}$$

where α is the hydrostatic stress sensitivity coefficient, which can be calculated from the relationship:

$$\alpha = 3 \frac{\tau_D}{\sigma_D} - \frac{3}{2}. \tag{24}$$

The fatigue limit for bending σ_D and torsion τ_D are material properties. For metals, the ratio $\frac{\tau_D}{\sigma_D}$ is usually close to $\frac{2}{3}$ (Fukuda and Nisitani, 2003). This ratio is used for the material of this paper with $\sigma_D = 50$ [MPa], giving $\tau_D \approx 33$ [MPa].
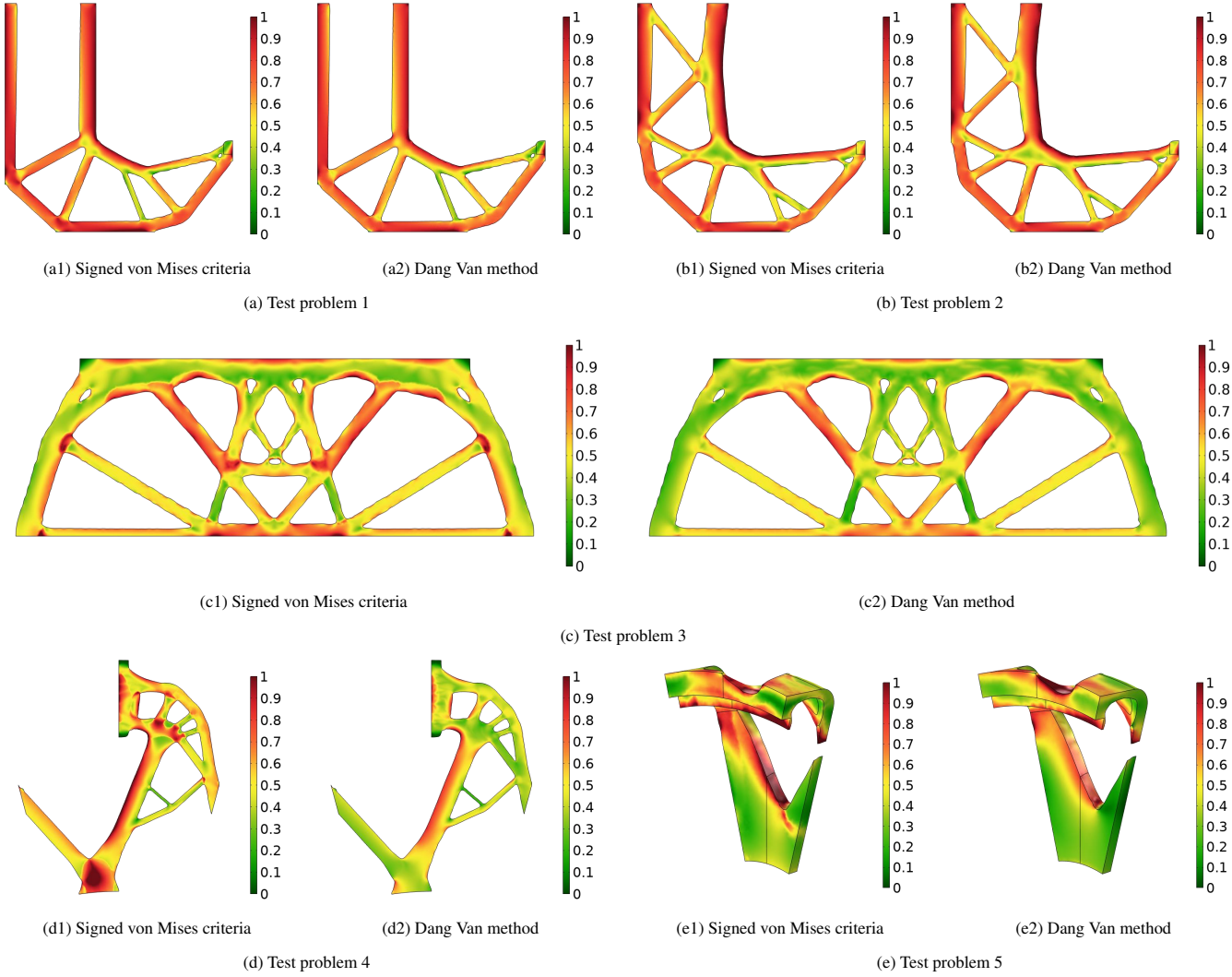
(a1) Signed von Mises criteria (a2) Dang Van method

(a) Test problem 1

(b1) Signed von Mises criteria (b2) Dang Van method

(b) Test problem 2

(c1) Signed von Mises criteria

(c2) Dang Van method

(c) Test problem 3

(d1) Signed von Mises criteria (d2) Dang Van method

(d) Test problem 4

(e1) Signed von Mises criteria (e2) Dang Van method

(e) Test problem 5

Figure 21: Validation of the normalized local fatigue constraints using the Dang Van critical plane method

From the results, shown in Figure 21, can be seen that for Test problems 1 & 2, the difference between the signed von Mises stress and Dang Van method is small. The difference between the two methods is more apparent in the succeeding analysed problems. Test problems 3, 4 & 5 show some regions that are critical using the signed von Mises stress, yet allowable according to the critical plane method. In these regions the sign of the hydrostatic stress suddenly shifts from positive to negative between time steps, which happens when the local stress is close to pure shear stress. This results in a significantly large stress variation that is an unrealistic representation of the reality. The signed von Mises stress has in previous research been shown to be less accurate when dealing with non-proportional loading for this reason (Papuga et al., 2012). Another notable difference is that the Dang Van method is less conservative for regions with a compresive mean stress. This is due to a difference in assumptions on the effect of mean stress between the two methods used. In Equation 14 of the method of this paper it was assumed that compresive mean stress does not affect the fatigue stress amplitude, whereas from Equation 23

can be seen that a negative hydrostatic stress reduces the fatigue criteria of the Dang Van method.

5. Conclusion & Recommendations

In this paper, a method has been presented to implement infinite fatigue life constraints in density based topology optimization for non-proportional loading problems as well as, in particular, cyclic symmetric problems. This combination did not exist and is practical for the design of rotating machinery, where cyclic symmetry is often seen. The method was used to minimize the mass of design problems in both 2D and 3D and in general black and white converged designs where found.

The method was first tested on several academic problems, where the non-proportional method was compared to a proportional approach, where proportional assumptions of the loading conditions were made. It was found that the non-proportional method could properly constrain the fatigue locally up to the accuracy of the constraint aggregation.

In contrast, the proportional approximations of the problems showed severe local violations of the fatigue constraint when subjected to the original non simplified loading. Although the studied examples did show that by making good assumptions, main topological features can be found, this is not always trivial and significant post processing would be necessary to obtain a final design which adheres to the constraints.

The non-proportional method also worked properly in combination with the enforced cyclic symmetry. Both a 2D and 3D problem have been analysed, where a single static FE-analysis provided respectively 12 and 13 time steps to the quasi-static analysis, significantly reducing the computation cost.

The Signed von Mises stress fatigue evaluation used is known to be inaccurate for regions where the sign of the hydrostatic stress suddenly changes in time. A critical plane method is more suitable for non-proportional loading fatigue evaluation and should be implemented into the method to improve final results.

Other recommendations are to incorporate new or existing methods to improve the constraint aggregation approximation, so that local constraint adherence is improved. Furthermore, the discontinuity in the modified Goodman correction, when the mean stress approaches the ultimate tensile strength, should be addressed and future research could also focus on suppressing the regions of intermediate density occasionally observed in moving load problems.

Appendix A. Manual design iteration to remove local stress peaks

A manual design iteration is made for the result of Test problem 1 to reduce the maximum constraint violations presumed to originate from numerical reasons or jagged interpreted boundaries. Where necessary, boundaries are manually redrawn using smooth curves while avoiding adding additional material. After the manual adjustment, the design is reanalyzed. The resulting maximum local fatigue for the proportional approach is 1.24307, as shown in Figure A.22, while only increasing the material usage by 0.51%. The resulting maximum local fatigue for the non-proportional approach is 1.18526, as shown in Figure A.23, with a material usage increase of 0.68%.
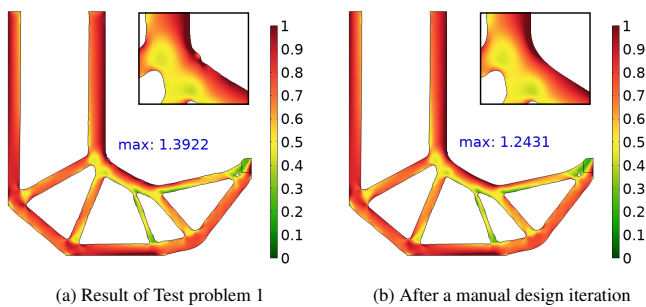
References

Amzallag, C., Gerey, J.P., Robert, J.L., Bahuaud, J., 1994. Standardization of the rainflow counting method for fatigue analysis. International Journal of Fatigue 16, 287–293. doi:10.1016/0142-1123(94)90343-3.

Barbarosie, C., Toader, A.M., 2010. Shape and topology optimization for periodic problems part ii: optimization algorithm and numerical examples. Structural and Multidisciplinary Optimization 40, 393–408. doi:10.1007/s00158-009-0377-1.

Bruggi, M., 2008. On an alternative approach to stress constraints relaxation in topology optimization. Structural and Multidisciplinary Optimization 36, 125–141. doi:10.1007/s00158-007-0203-6.

Bruns, T.E., Tortorelli, D.A., 2001. Topology optimization of non-linear elastic structures and compliant mechanisms. Computer Methods in Applied Mechanics and Engineering 190, 3443–3459. doi:10.1016/s0045-7825(00)00278-4.

Carpinteri, A., Spagnoli, A., Vantadori, S., 2017. A review of multiaxial fatigue criteria for random variable amplitude loads. Fatigue & Fracture of Engineering Materials & Structures 40, 1007–1036. doi:10.1111/FFE.12619.

Cheng, G., Jiang, Z., 1992. Study on topology optimization with stress constraints. Engineering Optimization 20, 129–148. doi:10.1080/03052159208941276.

Cheng, G.D., Guo, X., 1997. ϵ-relaxed approach in structural topology optimization. Structural Optimization 13, 258–266. doi:10.1007/bf01197454.

Choi, W.S., Park, G.J., 2002. Structural optimization using equivalent static loads at all time intervals. Computer Methods in Applied Mechanics and Engineering 191, 2105–2122. doi:10.1016/S0045-7825(01)00373-5.

Collet, M., Bruggi, M., Duysinx, P., 2017. Topology optimization for minimum weight with compliance and simplified nominal stress constraints for fatigue resistance. Structural and Multidisciplinary Optimization 55, 839–855. doi:10.1007/s00158-016-1510-6.

Cook, R.D., Malkus, D.S., Plesha, M.E., Witt, R.J., 2002. Concepts and applications of finite element analysis. 4 ed., John Wiley & Sons.

Duysinx, P., Bendsøe, M.P., 1998. Topology optimization of continuum structures with local stress constraints. International Journal for Numerical Methods in Engineering 43, 1453–1478. doi:10.1002/(SICI)1097-0207(19981230)43:8<1453::AID-NME480>3.0.CO;2-2.

Duysinx, P., Sigmund, O., 1998. New developments in handling stress constraints in optimal material distribution, in: 7th AIAA/USAF/NASA/ISSMO symposium on multidisciplinary analysis and optimization. doi:10.2514/6.1998-4906.

Fukuda, T., Nisitani, H., 2003. The background of fatigue limit ratio of torsional fatigue to rotating bending fatigue in isotropic materials and materials with clear-banded structure, in: European Structural Integrity Society. Elsevier. volume 31, pp. 285–302.

Giraldo-Londoño, O., Paulino, G.H., 2021b. Polydyna: a matlab implementation for topology optimization of structures subjected to dynamic loads. Structural and Multidisciplinary Optimization 64, 957–990. doi:10.1007/s00158-021-02859-6.

Hilber, H.M., Hughes, T.J., Taylor, R.L., 1977. Improved numerical dissipation for time integration algorithms in structural dynamics. Earthquake

| (a) Result of Test problem 1 | (b) After a manual design iteration |

Figure A.22: Reduced stress peaks after a manual design iteration for the proportional approach of Test problem 1.

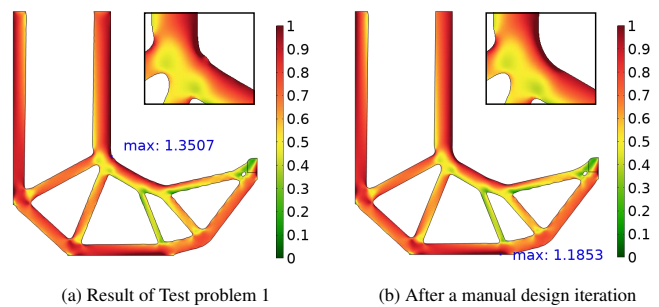| (a) Result of Test problem 1 | (b) After a manual design iteration |

Figure A.23: Reduced stress peaks after a manual design iteration for the non-proportional approach of Test problem 1.

Engineering & Structural Dynamics 5, 283–292. doi:10.1002/EQE.4290050306.

Holmberg, E., Torstenfelt, B., Klarbring, A., 2013. Stress constrained topology optimization. Structural and Multidisciplinary Optimization 48, 33–47. doi:10.1007/s00158-012-0880-7.

Holmberg, E., Torstenfelt, B., Klarbring, A., 2014. Fatigue constrained topology optimization. Structural and Multidisciplinary Optimization 50, 207–219. doi:10.1007/s00158-014-1054-6.

Huang, X., Xie, Y.M., 2008. Optimal design of periodic structures using evolutionary topology optimization. Structural and Multidisciplinary Optimization 36, 597–606. doi:10.1007/S00158-007-0196-1.

Jeong, S.H., Choi, D.H., Yoon, G.H., 2015. Fatigue and static failure considerations using a topology optimization method. Applied Mathematical Modelling 39, 1137–1162. doi:10.1016/J.APM.2014.07.020.

Jeong, S.H., Lee, J.W., Yoon, G.H., Choi, D.H., 2018. Topology optimization considering the fatigue constraint of variable amplitude load based on the equivalent static load approach. Applied Mathematical Modelling 56, 626–647. doi:10.1016/J.APM.2017.12.017.

Kang, B.S., Choi, W.S., Park, G.J., 2001. Structural optimization under equivalent static loads transformed from dynamic loads based on displacement. Computers & Structures 79, 145–154. doi:10.1016/S0045-7949(00)00127-9.

Karolczuk, A., Kluger, K., Łagoda, T., 2016. A correction in the algorithm of fatigue life calculation based on the critical plane approach. International Journal of Fatigue 83, 174–183. doi:10.1016/j.ijfatigue.2015.10.011.

Kosaka, I., Swan, C.C., 1999. A symmetry reduction method for continuum structural topology optimization. Computers & Structures 70, 47–61. doi:10.1016/S0045-7949(98)00158-8.

Lalanne, C., 2014. Mechanical Vibration and Shock Analysis, Fatigue Damage. volume 4. 3 ed., John Wiley & Sons.

Lazarov, B.S., Sigmund, O., 2011. Filters in topology optimization based on helmholtz-type differential equations. International Journal for Numerical Methods in Engineering 86, 765–781. doi:10.1002/NME.3072.

Le, C., Norato, J., Bruns, T., Ha, C., Tortorelli, D., 2010. Stress-based topology optimization for continua. Structural and Multidisciplinary Optimization 41, 605–620. doi:10.1007/s00158-009-0440-y.

Lee, J.W., Yoon, G.H., Jeong, S.H., 2015. Topology optimization considering fatigue life in the frequency domain. Computers & Mathematics with Applications 70, 1852–1877. doi:10.1016/J.CAMWA.2015.08.006.

Liu, H., Zhang, W., Gao, T., 2015. A comparative study of dynamic analysis methods for structural topology optimization under harmonic force excitations. Structural and Multidisciplinary Optimization 51, 1321–1333. doi:10.1007/s00158-014-1218-4.

Michaleris, P., Tortorelli, D.A., Vidal, C.A., 1994. Tangent operators and design sensitivity formulations for transient non-linear coupled problems with applications to elastoplasticity. International Journal for Numerical Methods in Engineering 37, 2471–2499. doi:10.1002/NME.1620371408.

Moses, E., Fuchs, M.B., Ryvkin, M., 2002. Topological design of modular structures under arbitrary loading. Structural and Multidisciplinary Optimization 24, 407–417. doi:10.1007/S00158-002-0254-7.

Oest, J., Lund, E., 2017. Topology optimization with finite-life fatigue constraints. Structural and Multidisciplinary Optimization 56, 1045–1059. doi:10.1007/s00158-017-1701-9.

Ottosen, N.S., Stenström, R., Ristinmaa, M., 2008. Continuum approach to high-cycle fatigue modeling. International Journal of Fatigue 30, 996–1006. doi:10.1016/J.IJFATIGUE.2007.08.009.

Papuga, J., Vargas, M., Hronek, M., 2012. Evaluation of uniaxial fatigue criteria applied to multiaxially loaded unnotched samples. Engineering Mechanics 19, 3.

Petrov, E.P., 2004. A method for use of cyclic symmetry properties in analysis of nonlinear multiharmonic vibrations of bladed disks. J. Turbomach. 126, 175–183. doi:10.1115/1.1644558.

Rao, J., 2011. History of rotating machinery dynamics. volume 20. Springer Science & Business Media.

Senhora, F.V., Giraldo-Londono, O., Menezes, I.F., Paulino, G.H., 2020. Topology optimization with local stress constraints: a stress aggregation-free approach. Structural and Multidisciplinary Optimization 62, 1639–1668. doi:10.1007/s00158-020-02573-9.

Sigmund, O., 2007. Morphology-based black and white filters for topology optimization. Structural and Multidisciplinary Optimization 33, 401–424. doi:10.1007/s00158-006-0087-x.

da Silva, G.A., Aage, N., Beck, A.T., Sigmund, O., 2021a. Local versus global stress constraint strategies in topology optimization: a comparative study. International Journal for Numerical Methods in Engineering 122, 6003–6036. doi:10.1002/nme.6781.

da Silva, G.A., Aage, N., Beck, A.T., Sigmund, O., 2021b. Three-dimensional manufacturing tolerant topology optimization with hundreds of millions of local stress constraints. International Journal for Numerical Methods in Engineering 122, 548–578. doi:10.1002/NME.6548.

Suresh, S., Lindström, S.B., Thore, C.J., Torstenfelt, B., Klarbring, A., 2020. Topology optimization using a continuous-time high-cycle fatigue model. Structural and Multidisciplinary Optimization 61, 1011–1025. doi:10.1007/s00158-019-02400-w.

Svanberg, K., 1987. The method of moving asymptotes—a new method for structural optimization. International Journal for Numerical Methods in Engineering 24, 359–373. doi:10.1002/NME.1620240207.

Svanberg, K., 2002. A class of globally convergent optimization methods based on conservative convex separable approximations. SIAM Journal on Optimization 12, 555–573. doi:10.1137/S1052623499362822.

Thomas, D.L., 1979. Dynamics of rotationally periodic structures. International Journal for Numerical Methods in Engineering 14, 81–102. doi:10.1002/NME.1620140107.

Verbart, A., Langelaar, M., van Keulen, F., 2017. A unified aggregation and relaxation approach for stress-constrained topology optimization. Structural and Multidisciplinary Optimization 55, 663–679. doi:10.1007/s00158-016-1524-0.

Wang, C.H., Brown, M.W., 1996. Life prediction techniques for variable amplitude multiaxial fatigue—part 2: comparison with experimental results. Journal of Engineering Materials and Technology 118, 371–374. doi:10.1115/1.2806822.

Wang, F., Lazarov, B.S., Sigmund, O., 2011. On projection methods, convergence and robust formulations in topology optimization. Structural and Multidisciplinary Optimization 43, 767–784. doi:10.1007/s00158-010-0602-y.

Yang, R.J., Chen, C.J., 1996. Stress-based topology optimization. Structural Optimization 12, 98–105. doi:10.1007/BF01196941.

Yoon, G.H., 2010. Structural topology optimization for frequency response problem using model reduction schemes. Computer Methods in Applied Mechanics and Engineering 199, 1744–1763. doi:10.1016/J.CMA.2010.02.002.

Zhang, S., Le, C., Gain, A.L., Norato, J.A., 2019. Fatigue-based topology optimization with non-proportional loads. Computer Methods in Applied Mechanics and Engineering 345, 805–825. doi:10.1016/J.CMA.2018.11.015.

Zhao, J., Wang, C., 2014. Robust topology optimization under loading uncertainty based on linear elastic theory and orthogonal diagonalization of symmetric matrices. Computer Methods in Applied Mechanics and Engineering 273, 204–218. doi:10.1016/j.cma.2014.01.018.

Zuo, Z., 2009. Topology optimization of periodic structures. Ph.D. thesis. RMIT University.

<div style="text-align: right; font-size: 3em;">4</div>

DOT design cases

The presented method has been applied to the two DOT cases. An additional challenge of these cases that became apparent was that allowable deformations were quite dominant constraints and had a significant influence on the optimized mass. These allowable deformations, however, were based on a FE-analysis of the whole drivetrain assembly and not very precise defined for the individual parts, especially when using simplified boundary conditions like the fixed support at the inner ring. Nevertheless, assumptions where made for these deformation constraints and applied. Approaches that where tried out to constrain displacements were either to constrain the mean compliance in time or to aggregate displacements on a specific surface where a specific maximum displacement was allowed. Since the global fatigue constraint underestimates the local fatigue constraints, a more conservative fatigue limit of $50\,[\mathrm{MPa}]$ as opposed to $60\,[\mathrm{MPa}]$ was used during the optimization, which means that the local constraints resulting from the optimization are satisfied according to the real fatigue limit for local fatigue amplitudes of $\frac{\sigma^{a0}}{\sigma_{\mathrm{D}}} \leq 1.2$.

4.1. DOT stator

For the DOT stator a target mass of $750\,[\mathrm{kg}]$ was specified for the full part. The assumed deformation constraint is a maximum allowable displacement at the load application surface. As a maximum displacement both $0.3\,[\mathrm{mm}]$ and $0.2\,[\mathrm{mm}]$ were used. The design domain is shown in Figure 4.1. The 2D model has an artificial thickness of $30\,[\mathrm{mm}]$
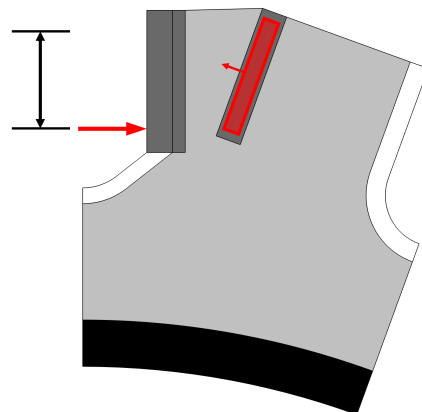

Figure 4.1: Design domain of the a stator segment. The black region is prescribed solid and fixed to the world. The dark gray regions are prescribed solid. A prescribed void region (white) is added along the boundary. A time-varying moving load is applied on the left boundary. A significantly smaller distributed load is applied on the prescribed solid section inside the light gray design domain.

The results of both optimizations are shown in Figure 4.2 and Figure 4.3 respectively. The total optimized mass obtained was $447\,[\mathrm{kg}]$ for the $0.3\,[\mathrm{mm}]$ constraint (40.4% below target) and $519\,[\mathrm{kg}]$ for a constraint of $0.2\,[\mathrm{mm}]$ (30.8% below target), which shows how sensitive the optimized design is to this non precise defined constraint. The two optimisations together do show a rough trend from which regions with potential mass reduction can be concluded. The local fatigue constraints for the real fatigue limit (1.2) were satisfied for both designs.
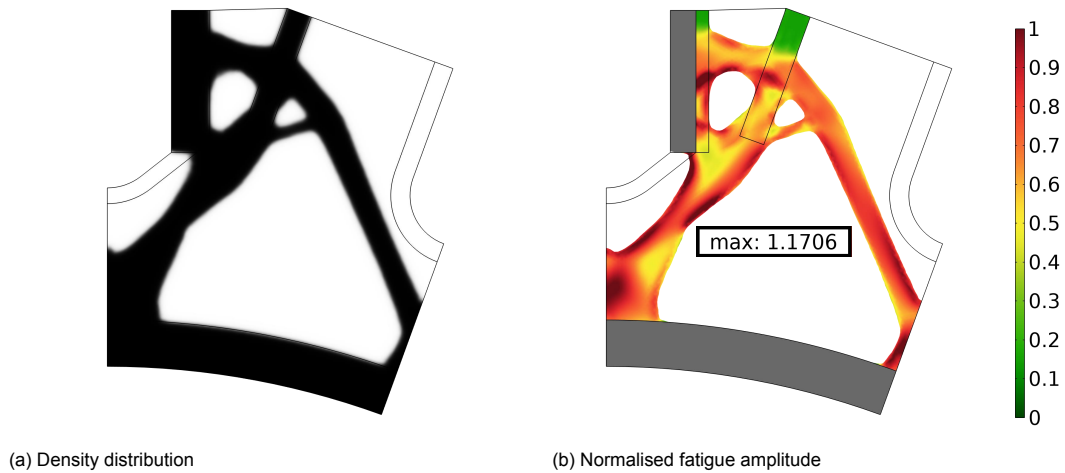

(a) Density distribution   (b) Normalised fatigue amplitude

Figure 4.2: Result of the optimized stator using a displacement constraint of $0.3\,[\mathrm{mm}]$.

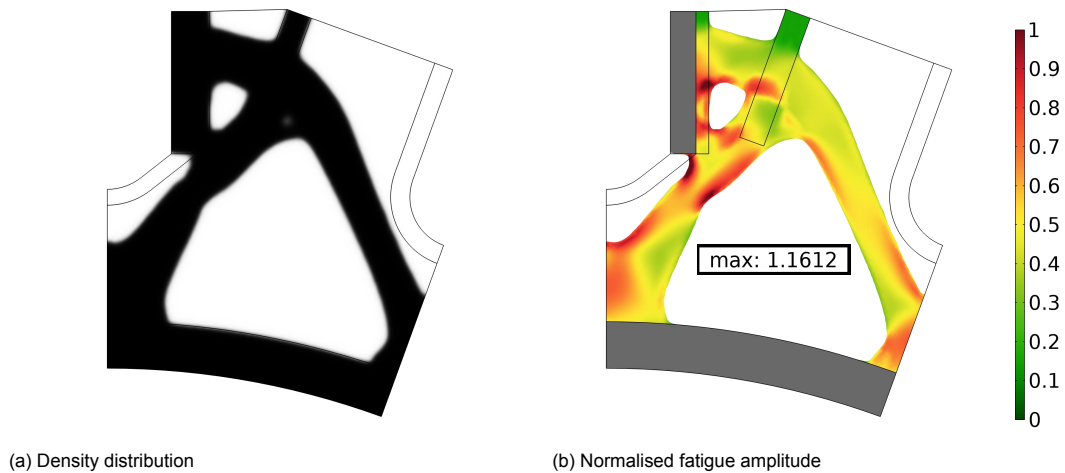(a) Density distribution   (b) Normalised fatigue amplitude

Figure 4.3: Result of the optimized stator using a displacement constraint of $0.2\,[\mathrm{mm}]$.

4.2. DOT rotor

The mass target of the rotor part was about $3000\,[\mathrm{kg}]$ excluding the cam ring. The deformation constraint of the rotor part was a lot more dominant than the allowable fatigue with respect to the material usage. A maximum axial displacement of $0.15\,[\mathrm{mm}]$ is prescribed on the inner ring and a maximum radial deformation of $0.3\,[\mathrm{mm}]$ on the cam ring. The design domain is shown in Figure 4.4.

From the results shown in Figure 4.5 can be seen that the fatigue is satisfied with respect to the real fatigue limit (1.2) and notably low throughout the structure. A mass of $2117\,[\mathrm{kg}]$ was obtained which is 29.4% smaller than the prescribed mass budget.
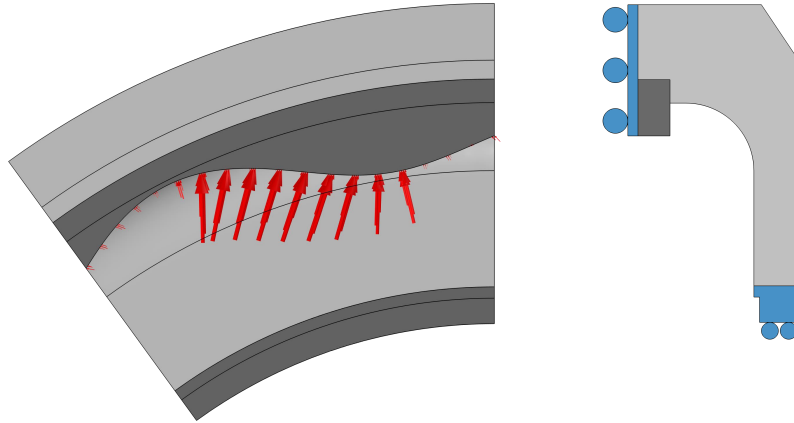
Figure 4.4: Design domain of the a rotor segment shown in light gray. The dark gray regions are prescribed solid. The inner ring can move freely in the axial direction. The left surface of the cam ring is constrained in the axial direction. A time-varying moving load is applied on the cam ring surface for which the different time steps are shown.
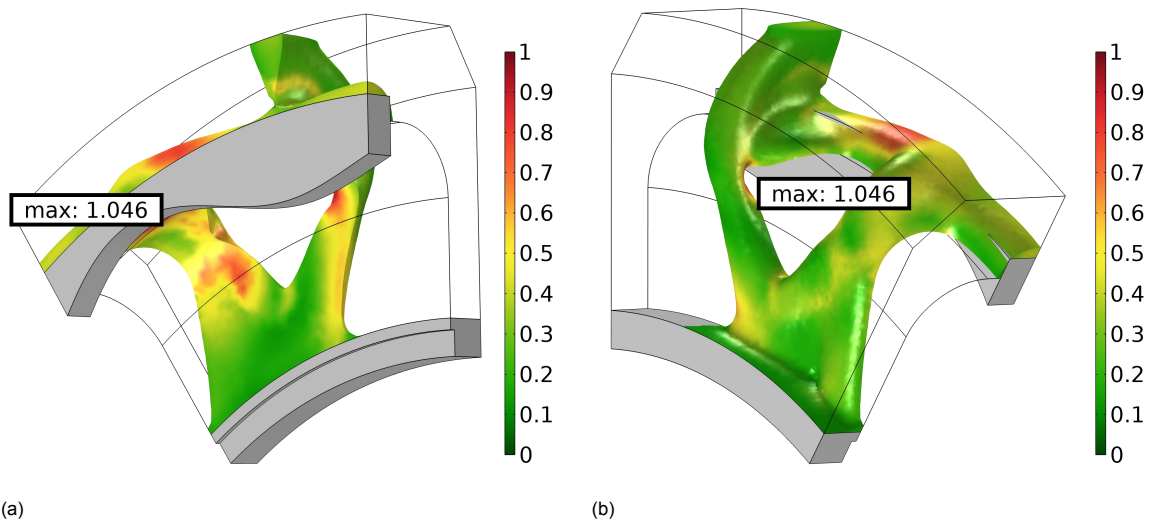

(a)   (b)

Figure 4.5: Normalised fatigue amplitude of the optimized rotor

4.3. Manufacturability

An additional structural requirement by DOT was the preference to construct the parts out of welded plates. For the 2D stator result obtained, which can be cut out from a plate, this should not be an issue. For the obtained rotor design however, the interpretation to a plate design is not trivial.

5

Discussion & Conclusion

5.1. Discussion

This section will give a brief discussion on the method presented in the article of Chapter 3. In general the final results of the examples analysed were black and white and convergence of the objective function was smooth. Some moving load problems, however, showed difficulty in fully eliminating gray regions. A possible explanation for this can be that the moving load can be considered as a distributed load over the range of motion. These remaining gray regions have been observed in previous research when dealing with distributed loads.

The results of Examples 2-5 show that when using the presented method, a fatigue constraint adherence can be achieved for non-proportional loading problems, that is comparable to the proportional problem Example 1. On the other hand, the proportional definitions of the problems showed severe local violations of the fatigue constraint. Depending on the quality of assumptions, the proportional approach was able to find main topological features in some cases. Making proper proportional assumptions of loading is, however, not always trivial and significant post processing would be necessary to obtain a final design which adheres to the constraints.

From the results of Examples 3-5, a disadvantage of using the signed von Mises stress as a fatigue criteria can be seen. Regions where the sign of the hydrostatic stress suddenly changes in time show exaggerated stress cycles which are an unrealistic representation of the reality. This effect is not always avoidable by changing the topology and can therefore show up as critical regions in the design, which most likely limit the optimization to further reduce the mass.

Using the method on the DOT design cases resulted in designs with considerably lower masses than the prescribed mass budget for the parts, while adhering to the fatigue requirements. However, it became apparent that the mass of the optimized result was very sensitive to the prescribed deformation constraints, which were not very precisely defined. The reliability of the structural optimum found is therefore debatable, but at the least it illustrated the potential of a significant mass reduction.

A preference was to construct the parts out of welded plates. Fatigue requirements around welds are generally more strict. To improve the manufacturability of the optimized design, a method could be developed that takes the plate design requirement into account, where more conservative regional fatigue constraints around weld locations are incorporated.

5.2. Conclusion

The goal of this work has been to presented a fatigue constrained topology optimization method to minimize the mass of cyclic symmetric structures subjected to non-proportional loading.

To evaluate infinite fatigue life for non-proportional loading, a quasi-static analysis is performed to obtain the time-varying stress history and a smooth min/max function is used to estimate the local largest stress cycles, which is differentiable and can therefore be implemented into TO.

33

The method was tested on some academic problems and compared to a proportional approach, where proportional assumptions of the loading conditions were made. It was found that the non-proportional method could properly constrain the fatigue for both 2D and 3D Test problems. The the proportional approach, on the other hand, showed severe violations.

It was found that cyclic symmetry can be exploited to reduce the computational cost of the quasi-static analysis. When the loading acting on each cyclic symmetric segment adheres to specified conditions, the static response of the whole structure can provide multiple time steps for the quasi-static analysis of a single segment through the responses of the other segments, significantly reducing the computational cost of the optimization problem.

5.2.1. Future work
The Signed von Mises stress fatigue evaluation used is known to be inaccurate for regions where the sign of the hydrostatic stress suddenly changes in time. A critical plane method is more suitable for non-proportional loading fatigue evaluation and should be implemented into the method to improve final results.

Another recommendations is to incorporate new or existing methods to improve the local constraint control, so that local constraint adherence is improved.

A last recommendation is to include a method which takes manufacturability constraints of a welded plate structure into account.

A
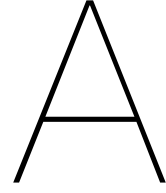
COMSOL implementation methods

In this appendix some of the less straight forward methods that were used for the implementation in COMSOL are discussed. It is, therefore, assumed that the reader is familiar with the basics of COMSOL.

A.1. Modeling a moving load

The distributed, moving loads are modeled using a Neumann type boundary condition (Sönnerlind 2016). This type of condition implements the load as a weak constraint on the selected boundary, as it is not possible to define a boundary mesh that fits the load distribution for all time points. The time-varying, moving load $\mathbf{f}(r(t), t)$ is defined as follows:

$$\mathbf{K}\mathbf{u}(t) = \mathbf{f}(r(t), t), \tag{A.1}$$

$$\mathbf{f}(r(t), t) = \begin{cases} \mathbf{f}(t), & \text{if } r(t) \leq a, \\ 0, & \text{otherwise,} \end{cases} \tag{A.2}$$

$$r(t) = \sqrt{(x - x(t))^2}. \tag{A.3}$$

Here, $\mathbf{K}$ and $\mathbf{u}(t)$ are the stiffness matrix and nodal displacements respectively. $x(t)$ is the time depending position of the loading as shown in Figure A.1 and $r(t)$ is a vector describing the absolute distance away from the loading. If the magnitude of the distance vector is smaller than the application width a, the distributed load $\mathbf{f}(t)$ is applied.

By defining $x(t), r(t)$ and a as variables, $\mathbf{f}(r(t), t)$ can be implemented as an if statement in a distributed boundary load.
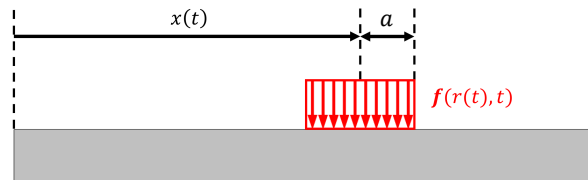

Figure A.1: An illustration of the variables used to model the moving load

A.2. Cyclic symmetry and quasi static analysis

The Cyclic symmetry and quasi static analysis is modeled using the linear extrusion function, which is a non local coupling that makes it possible to project variable fields of one geometry, onto a copy of that geometry as shown in Figure A.2. The density field of the copied segments are set to the projected density field of the design domain. The stress field is projected back to the design domain to construct the quasi static analysis.

$$\boldsymbol{\rho}$$

$$\boldsymbol{\sigma}(t_i)$$

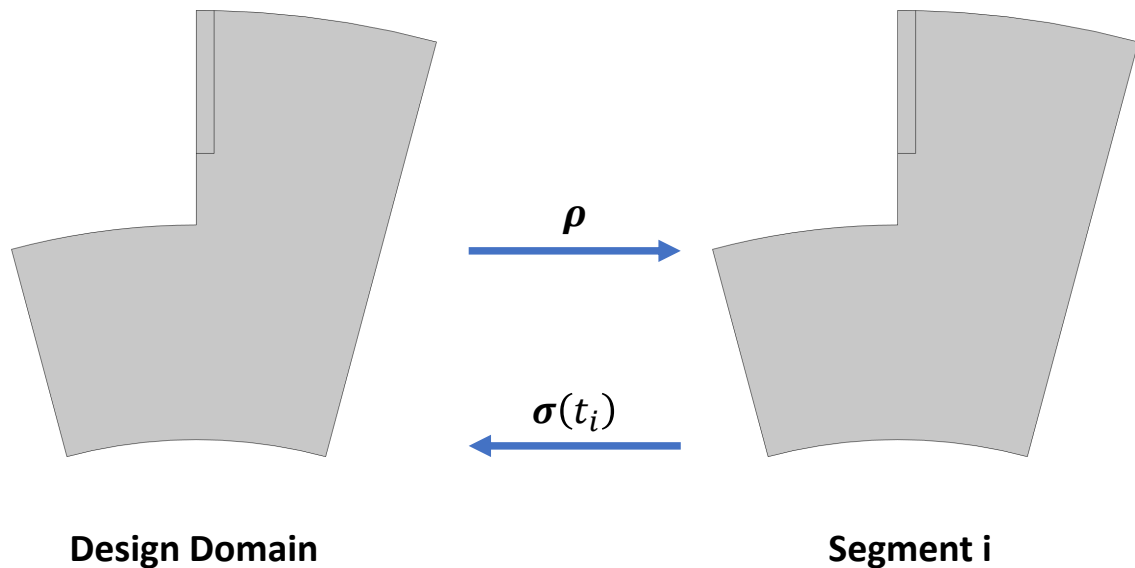**Design Domain**   **Segment i**

Figure A.2: Projection of densities and stress response between segments and design domain

A.3. Fatigue constraint

To implement the stress relaxation, the *equation view* option needs to be enabled. In the equation view option under the chosen material model of the solid mechanics, the stress relaxation can be applied to the individual elements of the stress matrix.

For the smooth maximum and minimum stress estimation in time, the linear extrusion function mentioned is used to sum the time step contributions of the design domain copies.

The lower bound aggregation function is implemented using the non local coupling average function.

A.3.1. Alternative approaches tried

Finding a method to implementing the smooth min/max estimation in time, in a way that was compatible with the TO study, was found to be quite a challenge. Several approaches were tried that did not work.

Firstly, using the withsol() operator to refer to the stress fields of different time steps, so that they can be summed in the smooth min/max function.

A second approach was to add the different time step contributions of the smooth min/max summation in a state variable.

Another approach was attempting to use the fatigue module study step into the TO study, which is a independent study step which evaluates fatigue from a FE-analysis input. The fatigue study did however not update between iterations.

The most promising approach that was tried was to integrate the time contributions of the smooth min/max function using the domain ODE interface. This approach was found to work for a compliance

minimization problem using the global ODE interface, but further investigation was abandoned when the linear extrusion approach was found to work for fatigue.

A.4. Using COMSOL Livelink for MATLAB

Implementing the method in COMSOL takes a lot of repetitive steps for each new case. To avoid mistakes and save time the Livelink with MATLAB can be used to adept the COMSOL model using MATLAB commands. This can help automate the set up of the linear extrusions and boundary conditions of the individual segments as well as apply changes in the model to all segments simultaneously. See the following example for commands that were used to set up the example problems studied. Text between <> require input that depends on the problem:

```matlab
1  segs = <number of segments>;
2
3  model = mphopen('<COMSOL_filename>');
4
5  %% Copy geometry
6  model.component('comp1').geom('geom1').create('copy1', 'Copy');
7  model.component('comp1').geom('geom1').feature('copy1').selection('input')
       .set({<geometry_to_copy>});
8  model.component('comp1').geom('geom1').feature('copy1').set('displx', <
       displacement>*[1:(segs-1)]);
9  model.component('comp1').geom('geom1').run('fin');
10
11 %%Copy meshing sequence
12 model.component('comp1').mesh('mesh1').feature('<mesh type>').selection.
       geom('geom1', 2);
13 model.component('comp1').mesh('mesh1').feature('<mesh type>').selection.
       set(<selection of original segment>);
14 model.component('comp1').mesh('mesh1').create('copy1', 'Copy');
15 model.component('comp1').mesh('mesh1').feature('copy1').selection('source'
       ).geom(2);
16 model.component('comp1').mesh('mesh1').feature('copy1').selection('
       destination').geom(2);
17 model.component('comp1').mesh('mesh1').feature('copy1').selection('source'
       ).set(<selection original segment>);
18 select = [];
19 for i = 1:(segs-1)
20     select = [select <selection of copy i>];
21 end
22 model.component('comp1').mesh('mesh1').feature('copy1').selection('
       destination').set(select);
23
24 %% Set up linear extrusions
25 for i = 1:(segs-1)
26 model.component('comp1').cpl.create(sprintf('linext%d',2*i-1), '
       LinearExtrusion');
27 model.component('comp1').cpl(sprintf('linext%d',2*i-1)).selection.set(<
       selection copy i >);
28 model.component('comp1').cpl(sprintf('linext%d',2*i-1)).selection('
       srcvertex1').set([<point 1 copy i>]);
29 model.component('comp1').cpl(sprintf('linext%d',2*i-1)).selection('
       srcvertex2').set([<point 2 copy i>]);
30 model.component('comp1').cpl(sprintf('linext%d',2*i-1)).selection('
       srcvertex3').set([<point 3 copy i>]);
31 model.component('comp1').cpl(sprintf('linext%d',2*i-1)).selection('
       dstvertex1').set([<point 1 original segment>]);
```

```matlab
32  model.component('comp1').cpl(sprintf('linext%d',2*i-1)).selection('
        dstvertex2').set([<point 2 original segment>]);
33  model.component('comp1').cpl(sprintf('linext%d',2*i-1)).selection('
        dstvertex3').set([<point 3 original segment>]);
34
35  model.component('comp1').cpl.create(sprintf('linext%d',2*i), '
        LinearExtrusion');
36  model.component('comp1').cpl(sprintf('linext%d',2*i)).selection.set(<
        selection segment 1>);
37  model.component('comp1').cpl(sprintf('linext%d',2*i)).selection('
        srcvertex1').set([<point 1 original segment>]);
38  model.component('comp1').cpl(sprintf('linext%d',2*i)).selection('
        srcvertex2').set([<point 2 original segment>]);
39  model.component('comp1').cpl(sprintf('linext%d',2*i)).selection('
        srcvertex3').set([<point 3 original segment>]);
40  model.component('comp1').cpl(sprintf('linext%d',2*i)).selection('
        dstvertex1').set([<point 1 copy i>]);
41  model.component('comp1').cpl(sprintf('linext%d',2*i)).selection('
        dstvertex2').set([<point 1 copy i>]);
42  model.component('comp1').cpl(sprintf('linext%d',2*i)).selection('
        dstvertex3').set([<point 1 copy i>]);
43  end
44
45  %% Set up density model
46  model.component('comp1').common('dtopo1').selection.set(<design domain
        selection>);
47  model.component('comp1').common('<optional features>').selection.set(<
        selection optional feature>);
48
49  for i= 1:(seg-1)
50  model.component('comp1').common.create(sprintf('ftopo%d',i), '
        FixedTopologyDomain');
51  model.component('comp1').common(sprintf('ftopo%d',i)).selection.set(<
        design domain copy i>);
52  model.component('comp1').common(sprintf('ftopo%d',i)).set('
        fixedDensityType', 'Custom');
53  model.component('comp1').common(sprintf('ftopo%d',i)).set('theta_fix',
        sprintf('linext%d(dtopo1.theta_c)',2*i));
54  end
55
56  %% Set up boundary conditions
57  model.component('comp1').physics('solid').feature('bndl1').selection.set(<
        selection on segment 1>);
58
59  model.component('comp1').variable.create('T1');
60  model.nodeGroup('grp1').add('variable', 'T1');
61  model.component('comp1').variable('T1').selection.geom('geom1', 2);
62  model.component('comp1').variable('T1').selection.set(<selection segment
        1>);
63  model.component('comp1').variable('T1').set('time', '1');
64
65  for i = 1:(steps-1)  %Exampele for a boundary load
66  model.component('comp1').physics('solid').create(sprintf('bndl%d',(i+1)),
        'BoundaryLoad', 1);
67  model.component('comp1').physics('solid').feature(sprintf('bndl%d',(i+1)))
        .selection.set(<selection on copy i>);
```

```
68  model.component('comp1').physics('solid').feature(sprintf('bndl%d',(i+1)))
        .set('LoadType', 'ForceLength');
69  model.component('comp1').physics('solid').feature(sprintf('bndl%d',(i+1)))
        .set('FperLength', {'if(r_t<a,f,0)' '0' '0'});
70
71  model.component('comp1').variable.create(sprintf('T%d',(i+1)));
72  model.nodeGroup('grp1').add('variable', sprintf('T%d',(i+1)));
73  model.component('comp1').variable(sprintf('T%d',(i+1))).selection.geom('
        geom1', 2);
74  model.component('comp1').variable(sprintf('T%d',(i+1))).selection.set(<
        selection copy i>);
75  model.component('comp1').variable(sprintf('T%d',(i+1))).set('time',
        sprintf('%d',i));
76  end
77
78  %% Set up constraints
79  model.component('comp1').variable.create('stress constraint');
80  model.component('comp1').variable.create('fatigue constraint');
81
82  local_stress_tmax = "exp(Snorm*k1)";      %Snorm = normalised von mises
        stress
83  local_Sstress_tmax = "exp(SSnorm*k1)";  %SSnorm = normalised signed von
        mises stress
84  local_Sstress_tmin = "exp(SSnorm*-k1)"; %K1 = aggregation parameter
85
86  for i = 1:(segs-1)
87  local_stress_tmax = append(local_stress_tmax,sprintf("+exp(linext%d(Snorm)
        *k1)",2*i-1));
88  local_Sstress_tmax = append(local_Sstress_tmax,sprintf("+exp(linext%d(
        SSnorm)*k1)",2*i-1));
89  local_Sstress_tmin = append(local_Sstress_tmin,sprintf("+exp(linext%d(
        SSnorm)*-k1)",2*i-1));
90  end
91
92  local_stress_tmax = append("log(",local_stress_tmax,")/k1");
93  local_Sstress_tmax = append("log(",local_Sstress_tmax,")/k1");
94  local_Sstress_tmin = append("log(",local_Sstress_tmin,")/-k1");
95  model.component('comp1').variable('stress constraint').set('
        local_stress_tmax', local_stress_tmax);
96  model.component('comp1').variable('fatigue constraint').set('
        local_Sstress_tmax', local_Sstress_tmax);
97  model.component('comp1').variable('fatigue constraint').set('
        local_Sstress_tmin', local_Sstress_tmin);
98
99  model.component('comp1').cpl('aveop1').selection.set(<selection on segment
         1 to aggregate>);
100
101 %% Save
102 mphsave(model,sprintf('<COMSOL_filename>_%dsegs',segs))
```
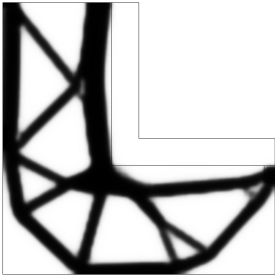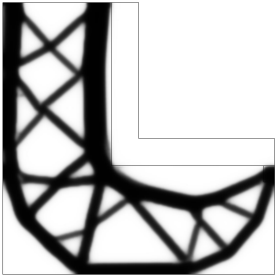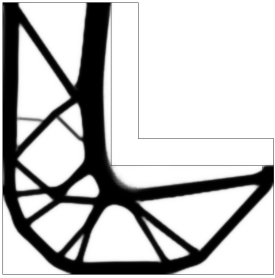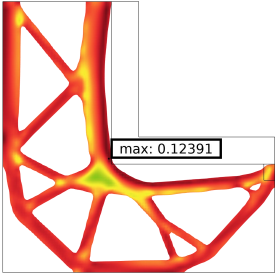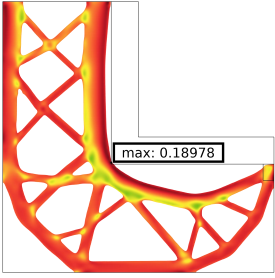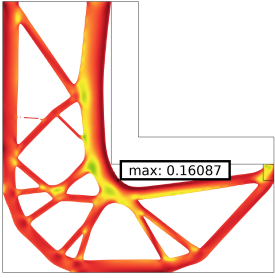
B

Mesh refinement and filter radius

The mesh size affects the solution in multiple ways. The increased number of elements result in a larger set of local constraints to aggregate. This lowers the accuracy of the aggregation function, as can be seen in Table B.1. Another way the mesh size influences the design is that it allows for a smaller filter radius, resulting in sharper boundaries, as can be seen in Table B.1. Due to the SIMP interpolation used on the material properties, the stresses found in the gray boundary are misrepresented. The sharper boundary increases the accuracy of the stresses in the structure.

Table B.1: The effect of the mesh size and filter radius R_{PDE} on the optimized design of Test problem 2.

Mesh $= 100 \times 100$, $R_{\mathrm{PDE}} = 1.5\,[\mathrm{mm}]$	Mesh $= 200 \times 200$, $R_{\mathrm{PDE}} = 1.5\,[\mathrm{mm}]$	Mesh $= 200 \times 200$, $R_{\mathrm{PDE}} = 0.75\,[\mathrm{mm}]$
$V = 0,4010$ $g^{\mathrm{f}}_{e,\max} = 0,12391$	$V = 0,4229$ $g^{\mathrm{f}}_{e,\max} = 0,18978$	$V = 0,3811$ $g^{\mathrm{f}}_{e,\max} = 0,16087$

Bibliography

Bendsøe, M. P. & Kikuchi, N. (1988), 'Generating optimal topologies in structural design using a homogenization method', *Computer Methods in Applied Mechanics and Engineering* **71**(2), 197–224. doi: 10.1016/0045-7825(88)90086-2.

Bendsøe, M. P. & Sigmund, O. (2003), *Topology optimization: theory, methods, and applications*, Springer Science & Business Media.

Bruggi, M. (2008), 'On an alternative approach to stress constraints relaxation in topology optimization', *Structural and Multidisciplinary Optimization* **36**(2), 125–141. doi: 10.1007/s00158-007-0203-6.

Cheng, G. D. & Guo, X. (1997), 'ϵ-relaxed approach in structural topology optimization', *Structural Optimization* **13**(4), 258–266. doi: 10.1007/bf01197454.

Cheng, G. & Jiang, Z. (1992), 'Study on topology optimization with stress constraints', *Engineering Optimization* **20**(2), 129–148. doi: 10.1080/03052159208941276.

DOT (2022), 'DOT3000 Power Train System (DOT3000 PTS) the development of a seawater-hydraulic drive train.'.
URL: *https://grow-offshorewind.nl/project/dot3000-pts*

Duysinx, P. & Bendsøe, M. P. (1998), 'Topology optimization of continuum structures with local stress constraints', *International Journal for Numerical Methods in Engineering* **43**(8), 1453–1478. doi: 10.1002/(SICI)1097-0207(19981230)43:8<1453::AID-NME480>3.0.CO;2-2.

Duysinx, P. & Sigmund, O. (1998), 'New developments in handling stress constraints in optimal material distribution', *In: 7th AIAA/USAF/NASA/ISSMO symposium on multidisciplinary analysis and optimization* pp. 1501–1509. doi: 10.2514/6.1998-4906.

Le, C., Norato, J., Bruns, T., Ha, C. & Tortorelli, D. (2010), 'Stress-based topology optimization for continua', *Structural and Multidisciplinary Optimization* **41**(4), 605–620. doi: 10.1007/s00158-009-0440-y.

Sönnerlind, H. (2016), 'How to make boundary conditions conditional in your simulation'.
URL: *https://www.comsol.com/blogs/how-to-make-boundary-conditions-conditional-in-your-simulation/*

Yang, R. J. & Chen, C. J. (1996), 'Stress-based topology optimization', *Structural Optimization* **12**(2), 98–105. doi: 10.1007/BF01196941.